

1 The landscape of transcriptional and translational changes over 22 2 years of bacterial adaptation

3 John S. Favate^{1,*}, Shun Liang¹, Srujana S. Yadavalli^{1,3}, Premal Shah^{1,2,*}

4

5 ¹ Department of Genetics, Rutgers University, Piscataway NJ, USA

6 ² Human Genetics Institute of New Jersey, Rutgers University, Piscataway NJ, USA

7 ³ Waksman Institute, Rutgers University, Piscataway NJ USA

8 *Correspondence: premal.shah@rutgers.edu, john.favate@rutgers.edu

9

10 Abstract

11 Organisms can adapt to an environment by taking multiple mutational paths. This redundancy at the
12 genetic level, where many mutations have similar phenotypic and fitness effects, can make untangling the
13 molecular mechanisms of complex adaptations difficult. Here we use the *E. coli* long-term evolution
14 experiment (LTEE) as a model to address this challenge. To bridge the gap between disparate genomic
15 changes and parallel fitness gains, we characterize the landscape of transcriptional and translational changes
16 across 11 replicate populations evolving in parallel for 50,000 generations. By quantifying absolute changes
17 in mRNA abundances, we show that not only do all evolved lines have more mRNAs but that this increase in
18 mRNA abundance scales with cell size. We also find that despite few shared mutations at the genetic level,
19 clones from replicate populations in the LTEE are remarkably similar to each other in their gene expression
20 patterns at both the transcriptional and translational levels. Furthermore, we show that the bulk of the
21 expression changes are due to changes at the transcriptional level with very few translational changes.
22 Finally, we show how mutations in transcriptional regulators lead to consistent and parallel changes in the
23 expression levels of downstream genes, thereby linking genomic changes to parallel fitness gains in the
24 LTEE. These results deepen our understanding of the molecular mechanisms underlying complex
25 adaptations and provide insights into the repeatability of evolution.

26

27 Introduction

28 Comparative genomic approaches and large scale mutation experiments have allowed us to map
29 genetic changes to phenotypic changes underlying adaptation in many cases involving individual genes such
30 as hemoglobin¹, hormone receptors², and influenza proteins^{3,4}. However, when organisms adapt to novel
31 environments such as during yeast evolution under nutrient limitation⁵⁻⁷, adaptation to high-temperature
32 stress⁸, bacterial evolution during infections⁹, and long-term adaptation of *Escherichia coli* to minimal media¹⁰⁻
33 ¹³, genomic changes are widespread. Understanding how these changes lead to functional changes at the
34 molecular level is critical to understand the mechanistic basis of adaptations.

35

36 Here we use the *E. coli* long-term evolution experiment as a model system to characterize the
37 mechanistic basis of adaptation to a novel environment. Recent studies using LTEE have quantified the
38 dynamics of fitness growth¹⁴, identified the proportion of beneficial mutations¹², characterized mutational
39 dynamics in the system¹³, and identified the mechanistic basis of specific adaptations such as citrate
40 utilization in Ara-3¹⁵. Despite significant contributions to the understanding of adaptation in the LTEE, the role
41 that changes in transcription and translation play in increasing growth rates remains unexplored. An earlier
42 study of gene expression changes in LTEE showed parallel changes in transcription profiles in two of the
43 twelve evolved lines, Ara-1 and Ara+1, at 20,000 generations using radioactive microarrays¹⁶. Whether
44 parallelism in gene expression changes extends to the other lines and persists over a more extended period
45 remains unknown. Furthermore, since changes at the transcriptional level can be buffered at the translational
46 level^{17,18}, changes to both must be considered. Finally, significant changes in cell-size and morphology of the
47 bacteria^{19,20} over the course of adaptation indicate a need to quantify both relative and absolute changes in
48 expression.

49

50 Results

51 To address these questions, we performed RNA-seq and ribosomal footprinting (also called Ribo-
 52 seq)²¹ in the exponential phase of the ancestral strains and single clones from each of the 12 evolved lines
 53 at 50,000 generations (Fig. 1A). We analyzed single clones from Tenailon et al. 2016 and considered 4216
 54 protein-coding genes from the ancestors. We aligned sequencing data for each evolved clone to its unique
 55 genome. We restricted our analysis to 11 out of 12 evolved lines due to ancestral contamination in one of our
 56 samples (Ara+6). We averaged between 151 and 1693 reads per gene across the 52 libraries (Fig. S1A,
 57 Table S1). The distributions of read counts per gene were similar across lines, replicates, and sequencing
 58 methods (Fig S1C). We also observed a clear three-nucleotide periodicity in our Ribo-seq datasets (Fig. S1B,
 59 Table S2).

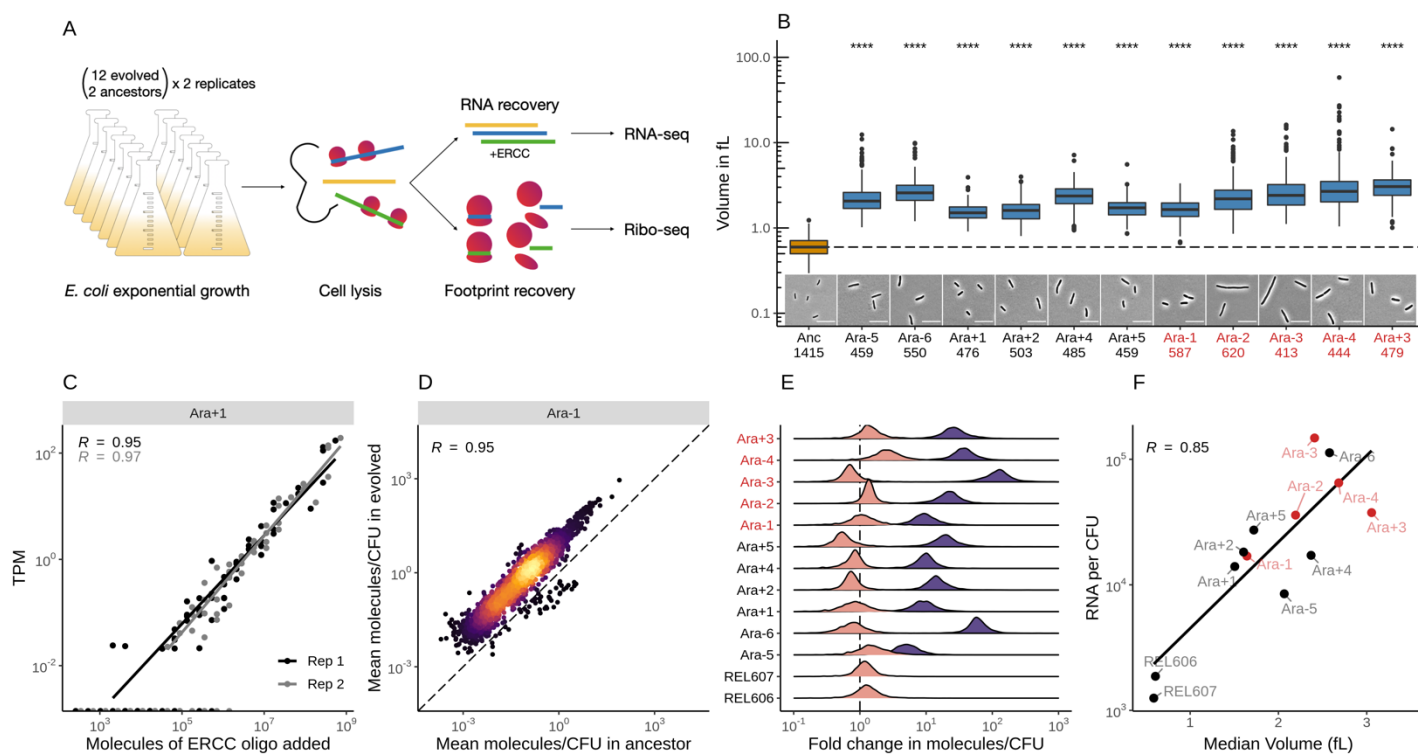
60

61 Evolved lines are larger and carry more mRNAs

62 Contrary to expectations, every evolved line in the LTEE has become larger in size compared to the
 63 ancestor^{19,20,22}. While bacterial size (cell volume) is a function of its growth rate, which typically depends on
 64 nutrient availability^{23–25}, the increase in cell size in LTEE²³ is not entirely a consequence of faster growth rate¹⁹.
 65 This increase appears to be under selection and is partly caused by mutations in Penicillin-binding protein
 66 genes, which also led to the increased circularity of the cells²⁶. Moreover, cultures of the evolved lines were
 67 recently found to have higher biomass with proportionally higher amounts of nucleic acids compared to the
 68 ancestors²⁷. Because changes to cell volume can affect transcription rates and alter relative concentrations
 69 of RNA molecules²⁸, we chose to quantify changes in the absolute abundance of mRNAs.

70

71 We used phase-contrast microscopy to measure the size and shape of cells in each of the ancestral
 72 and evolved lines and calculated cell volume based on these measurements (see methods, Table S3). We
 73 find that each evolved line has a larger volume than the ancestor (Welch's t-test, $p < 0.0001$ for all lines) (Fig.
 74 1B). We also find that evolved lines form filaments more frequently and formed longer filaments than the
 75 ancestor (see Supplementary Analysis). However, the larger size of evolved lineages is not entirely due to
 76 higher filamentation. Even after filtering out filaments (cells $>3x$ median volume), all evolved lines were still
 77 significantly larger compared to the ancestor (Welch's t-test, $p < 0.0001$ for all lines) (Fig. S2B).



78

79 Figure 1: **A.** Schematic of the experimental design. **B.** All evolved lines are larger than the ancestral strain.
80 Distributions of cellular volume as determined by phase-contrast microscopy and assuming spherocylindrical
81 shape of *E. coli* along with representative images for each line. Numbers underneath a line's name indicates
82 the total number of cells imaged (scale bar is 10 μ m, see Figure S3 for representative images.). The dashed
83 line indicates the ancestral median, p-values indicate the results of a t-test when each line is compared to the
84 ancestor, **** p \leq 0.0001. Lines listed in red have mutator phenotypes. **C.** Spike-in RNA control abundances
85 are correlated with their estimates in sequencing data. Linear models relating the number of molecules of
86 each ERCC control sequence added to their RNA-seq TPM (transcripts per million) in Ara+1 RNA-seq
87 samples (see Fig. S4 for all lines). **D.** Most genes have a higher absolute expression in evolved lines. Changes
88 in the absolute number of mRNA molecules per CFU (colony forming unit) in the 50,000th generation of Ara+1
89 relative to the ancestor. The values plotted are the average between 2 replicates of the evolved lines and
90 both replicates from both ancestors (REL606 and REL607; see Fig. S4 for all lines). **E.** Absolute changes in
91 mRNA abundances in evolved lines are significantly larger than the variation between biological replicates (t-
92 test, p < .0001 in all cases). Distributions of fold-changes of mRNA molecules per CFU. Pink curves indicate
93 gene-specific fold-changes between biological replicates for each line (centered around 1). Purple curves
94 show the fold-change from the 50,000th generation of an evolved line to the ancestor. Fold-change was
95 calculated in the same manner as in D. **F.** Larger evolved lines have more mRNA per CFU. Relationship
96 between the median volume for each line and the total number of RNA molecules per CFU for each line. Total
97 molecules of RNA are calculated as the sum of the average number of molecules for each gene between
98 replicates.

99

100 To measure how changes in cell size affect absolute RNA abundances, we measured the number of
101 colony-forming units (CFU) that went into each library (Table S4). We added the ERCC RNA spike-in
102 controls²⁹, a set of 92 RNA oligos in known amounts, to our RNA-seq libraries (table S5). This allowed us to
103 quantify the number of molecules per CFU for each transcript. We find a linear relationship between the
104 number of molecules of ERCC oligos and the number of transcripts quantified using RNA-seq (TPM) (Fig.
105 1C, S4A). Fold-changes in absolute counts ranged widely in each of the lines (Fig. 1E, Table S6) but were
106 overwhelmingly greater than one. Moreover, the increase in mRNA abundances in evolved lines relative to
107 the ancestor were greater than differences in abundances between corresponding biological replicates (Fig.
108 1E, t-test, p < .0001 in all cases). This suggests that all evolved lines have more mRNA molecules compared
109 to the ancestral strains. Finally, we show that evolved lineages with larger cells have more mRNAs (Fig. 1F),
110 suggesting that absolute abundances of mRNAs scale with cell size.

111

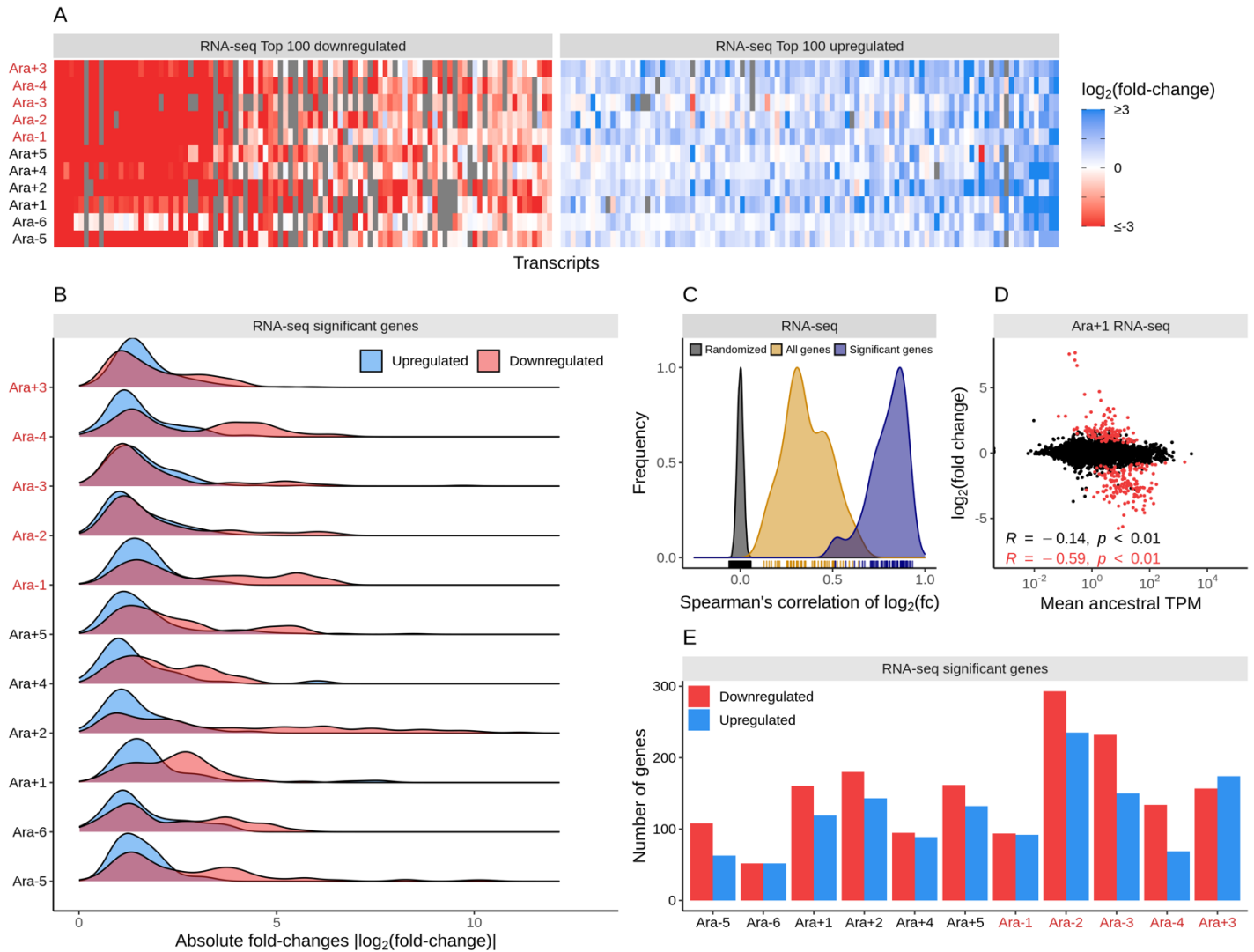
112 **Gene expression changes are parallel at both transcriptional and translational levels**

113 Despite a high degree of parallelism in fitness, few mutations are shared across the evolved lineages,
114 and each of the lines was founded on a unique set of mutations¹². At the gene level, only 57 genes have
115 mutations in two or more lines¹². Moreover, it remains unclear if the functional effects of these mutations are
116 similar across lines. To bridge the weak parallelism at the genotypic level with the strong parallelism at the
117 fitness level, we took gene expression as a molecular phenotype and quantified transcription and translation.
118 Earlier radioactive microarray-based experiments with two evolved lineages (Ara+1 and Ara-1) at 20,000
119 generations have showed that the expression patterns between the two evolved lines were more similar to
120 each other than either were to the ancestor¹⁶. However, it remains unclear if the pattern of parallel gene
121 expression changes is identical across all evolved lineages and has remained mostly parallel over a more
122 extended period.

123

124 We find that expression levels of genes were surprisingly similar across evolved lineages. Pairwise
125 correlations based on TPM showed a high degree of similarity among the evolved lines for RNA-seq and
126 Ribo-seq datasets (Fig. S5A, Table S1). Interestingly, pairwise correlations between evolved lines were not
127 significantly different from correlations between evolved lines and the ancestors (Fig. S5B). This suggests

128 that expression patterns of many genes remained mostly unchanged over 50,000 generations. We then
 129 sought to systematically quantify the degree of expression changes in both RNA-seq and Ribo-seq datasets
 130 using DESeq2³⁰ in each of the evolved lines (Table S7). Overall, half of all genes across all lines had less
 131 than a 30% change in their expression levels (Fig. S5C). However, several genes showed large changes in
 132 their expression patterns that varied by a thousand-fold (\log_2 fold-change > 10).
 133

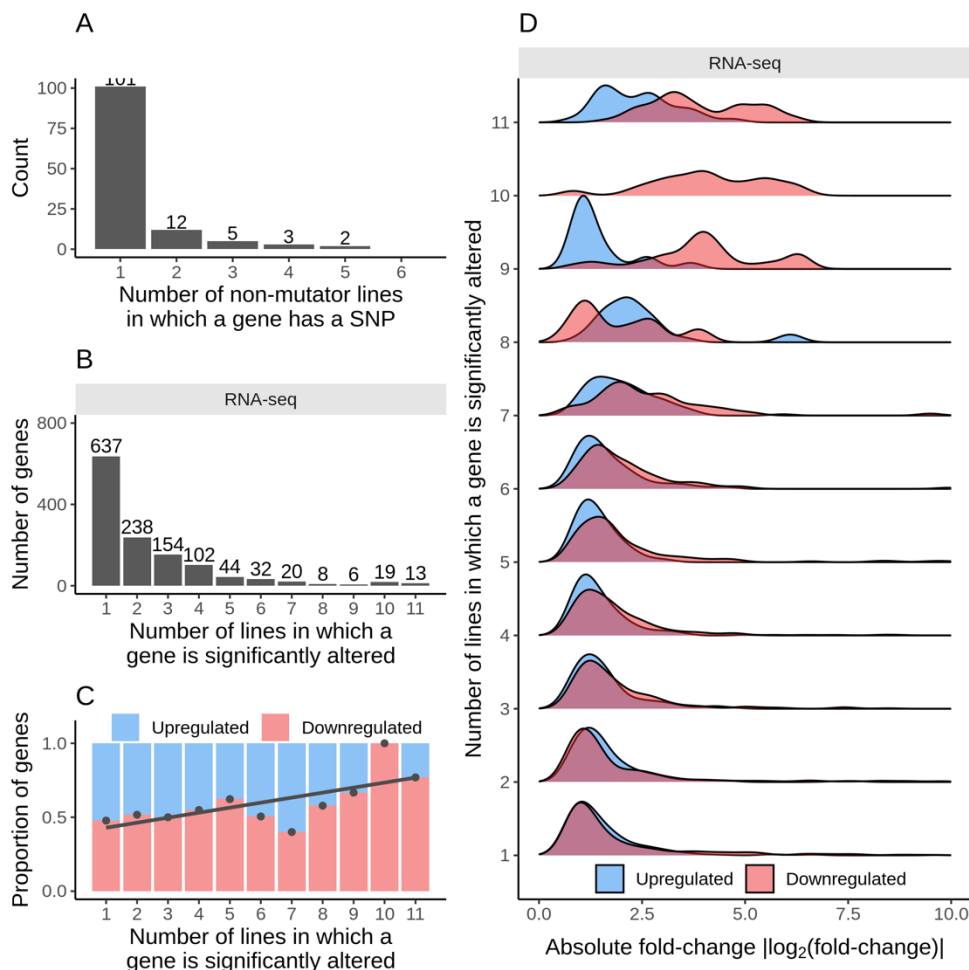


134
 135
 136
 137
 138
 139
 140
 141
 142
 143
 144
 145
 146
 147
 148

Figure 2: **A**. Parallelism in expression changes across evolved lines. The fold-changes of top 100 down and upregulated genes in each of the lines in the RNA-seq datasets. Genes are ordered from left to right in order of increasing mean fold-change across evolved lines. Gray bars represent gene deletions. **B**. Downregulated genes have larger effect sizes than upregulated genes. Distribution of statistically significant fold-changes in each line. Statistical significance was based on DESeq2 results using $q \leq 0.01$. **C**. Pairwise correlations of evolved lines based on all (yellow curve) or only statistically significant (blue curve) RNA-seq fold-changes. Each of these curves is significantly different from a distribution based on correlations made after randomizing the fold-changes (grey curve) within each line ($p \leq 0.01$, t-test). **D**. Fold-changes in expression levels of genes in evolved lines scale negatively with their ancestral expression levels. The relationship between ancestral TPM in the RNA-seq dataset and RNA-seq fold-change in Ara+1. The red dots represent significantly altered genes, and the black dots represent the remaining genes. **E**. The number of significantly down and upregulated genes in each line.

149
150
151
152
153
154
155
156
157
158
159
160

We find a high degree of parallelism in expression changes at both the transcriptional and translational levels (Fig. 2 and S6). The top 100 up and downregulated genes (defined as having the largest mean positive or negative fold-change across the evolved lines) showed remarkably similar fold-changes (RNA-seq, Fig. 2A; Ribo-seq, Fig. S6A). Distributions of all pairwise comparisons of fold-changes in evolved lines showed positive correlations, which became even more positive when considering only statistically significant genes (RNA-seq, Fig. 2B; Ribo-seq, Fig. S6D). Interestingly, we find that a higher number of genes were downregulated than upregulated across most lines (RNA-seq, Fig. 2E; Ribo-seq, Fig S6C). Moreover, the magnitude of downregulations was larger than that of upregulations in all but Ara+3 (Welch's t-test, $p < 0.05$ in all cases) (RNA-seq, Fig. 2B; Ribo-seq, Fig S6B). Surprisingly, evolved lines arrived at similar transcriptional and translational profiles regardless of whether they had a mutator phenotype or not (Fig. S6E).



161
162
163
164
165
166
167
168
169
170
171
172

Figure 3: **A**. The number of non-mutator lines in which a gene has at least one SNP inside the coding sequence. **B**. The number of evolved lines in which a gene's expression level was significantly altered ($q \leq 0.01$) was based on the DESeq2 results for RNA-seq datasets. **C**. Frequently altered genes are typically downregulated. The proportion of up and downregulated genes as a function of their frequency of expression changes across lines. **D**. Frequently downregulated genes have larger effect sizes than upregulated genes. Distributions of the RNA-seq fold-changes for the genes in the x-axis categories of C.

We next examined if changes in expression levels of a gene were somehow related to their expression in the ancestor. When we considered all genes, we observed a weak negative relationship between ancestral TPM and fold-change in an evolved line (Fig. 2D, S6F). This negative relationship is likely a by-product of the overall increase in mRNA abundances with cell-size. Due to biophysical constraints, genes with high ancestral

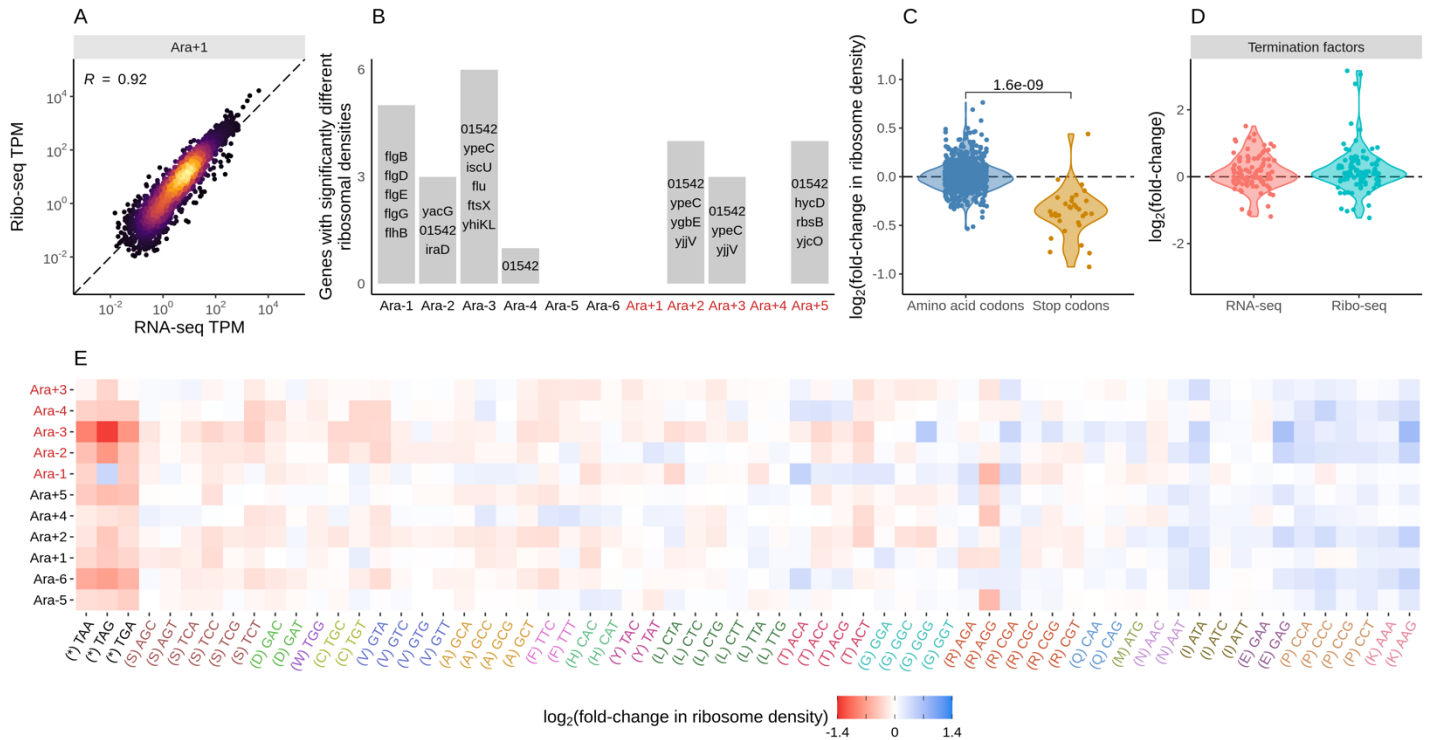
173 expression are unlikely to see large increases in mRNA abundances relative to genes with low expression.
174 As a result, genes with low ancestral mRNA abundances appear more upregulated when considering only
175 relative expression levels. However, when only statistically significant genes were considered, we see a very
176 strong negative relationship in most lines. The slope of this relationship is distinctly more negative than for all
177 genes. Additionally, the proportions of significantly upregulated genes decreased with the ancestral gene
178 expression level for most lines (Fig. S6G).

179
180 We observed high levels of parallelism in expression changes despite few shared mutations across
181 multiple lines (Fig. 3A, Table S8). We find that both the proportions of downregulated genes and their
182 magnitude of downregulation increased with the number of lines a gene was significantly altered in (Fig. 3C
183 and D), indicating that more downregulations were shared across lines than upregulations. This implies that
184 there are fewer genes and pathways whose downregulation increases fitness, whereas genes and pathways
185 whose expression increases enable higher fitness are more varied and unique to each line. We find similar
186 patterns for the Ribo-seq datasets (Fig. S7).

187 188 **Transcriptional changes drive translational changes**

189 Translational regulation affects the rate at which an mRNA produces its protein product. Different
190 mRNAs are translated with varying efficiencies in both eukaryotes and prokaryotes^{21,31,32}. However, the role
191 of changes in translational regulation during adaptation and speciation remains poorly understood and is
192 heavily debated^{18,33}. To study translational changes, we performed high-throughput ribosome-footprinting in
193 both the evolved lines and their ancestors.

194
195 Interestingly, we find that gene-specific ribosome-footprint abundances were highly correlated with
196 mRNA abundances ($R \geq 0.92$ for all lines, Fig. 4A and S8A). Since the number of ribosome-footprints from a
197 gene also depends on its mRNA abundances, we used Riborex³⁴ to evaluate gene-specific changes in
198 ribosomal-densities in each of the evolved lines relative to the ancestor. Surprisingly, we find very little
199 evidence of translational changes (Fig. 4B, Table S9). The number of genes with significantly altered ($q \leq$
200 0.01) ribosome-densities ranged from 0-6 genes across all lines, with a total of only 18 unique genes showing
201 altered ribosome-densities. Overall, changes in ribosome-densities on transcripts were sparse, suggesting
202 that transcriptional changes are the dominant force behind expression changes in the LTEE.



203

204

205

206

207

208

209

210

211

212

213

214

215

216

217

218

219

220

221

222

223

224

225

226

227

228

229

230

231

232

Figure 4: **A.** Translational changes are positively correlated with transcriptional changes. The relationship between RNA-seq and Ribo-seq TPM in Ara+1. The TPMs are averaged between the replicates. **B.** The distribution and identity of genes with significantly altered ribosomal densities ($q \leq 0.01$). **C.** Evolved lines have faster translation termination. Stop codons had lowered ribosome density compared to amino acid codons. Each point represents a stop codon from an evolved line, and the y-axis is fold-change in ribosomal density relative to the ancestor. P-value based on a t-test. **D.** Fold-changes in expression levels of translation termination factors and related genes *ykfJ*, *prfH*, *prfA*, *prmC*, *prfB*, *fusA*, *efp*, *prfC*. **E.** Changes in codon-specific ribosome densities in each of the evolved lines relative to the ancestor. Codons are arranged from left to right in order of increasing mean fold-change for their respective amino acid across the lines.

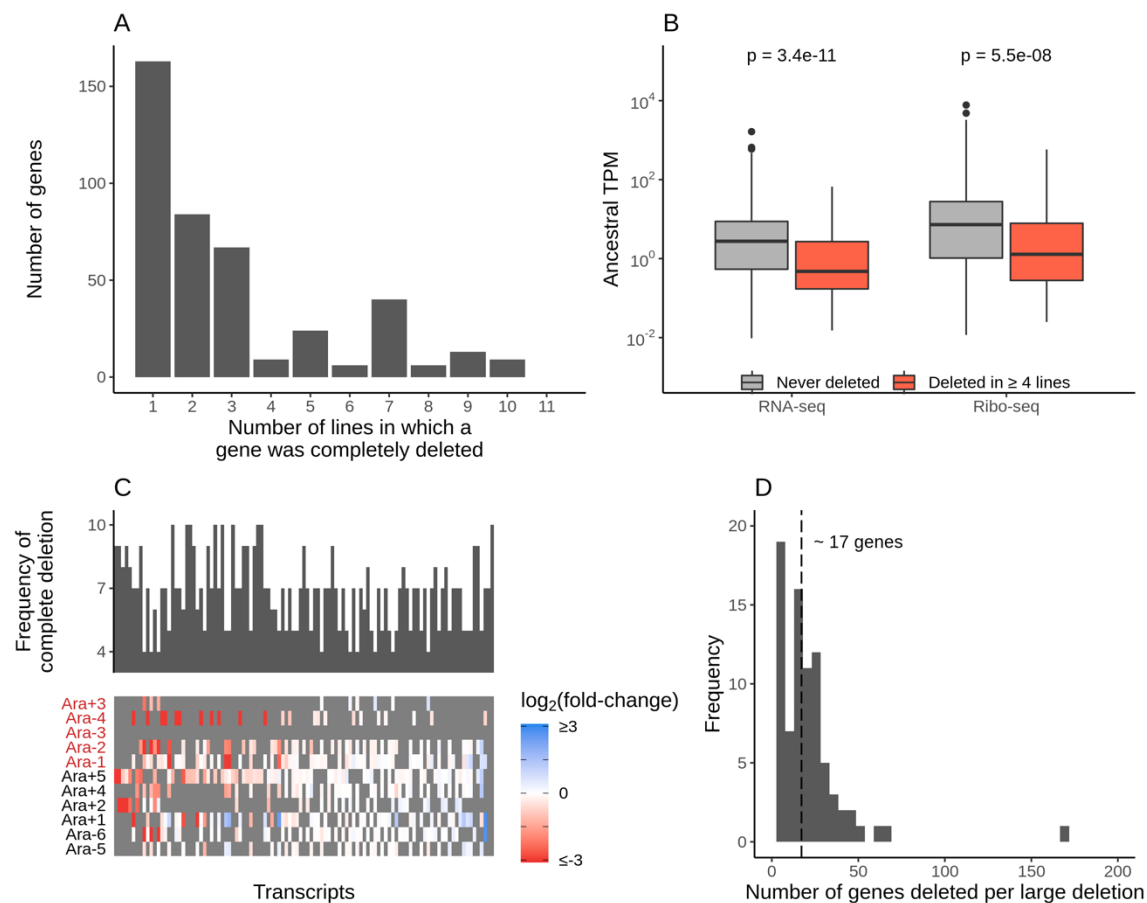
While ribosome-density changes reflect changes to the overall number of ribosomes per transcript, they do not reveal information about the translation of specific codons or amino acids. We find that the ribosome-densities at stop codons were significantly lower in all the evolved lines than in the ancestors (Fig. 4C and 4E, Table S10), suggesting that translation termination was significantly faster in evolved lines. Translation initiation and termination are relatively slow processes compared to elongation. As a result, faster termination might be adaptive in that it allows faster recycling of ribosomes, thereby increasing overall protein synthesis rates. Furthermore, we reasoned that this change in stop-codon ribosome-densities might be due to changes in expression levels of proteins that aid translation termination, such as release factors. We examined changes in genes related to termination, namely *frr* (ribosome recycling factor³⁵), *fusA* (elongation factor G³⁶), *prfABC* (peptide release factors A, B, C^{37,38}), and *prmC* (a methylase required for the function of *prfAB*³⁹). These genes showed differing directions and magnitudes of alteration at the RNA level, and these changes were rarely statistically significant (Fig. 4D, S8C). *prfB* and *prfC* facilitate the release of a protein from the ribosome at a stop codon and were typically upregulated, indicating an increase in their expression might be responsible for faster translation termination.

We also find higher ribosome-densities at Proline codons across all lines, indicating that elongation rates at these codons have slowed. Given this apparent slowdown at proline codons, we examined if genes involved in proline biosynthesis had altered expression levels. However, the three enzymes directly involved in proline biosynthesis - *proA*, *proB*, and *proC*, the proline tRNA ligase - *proS*, and elongation factor P involved

233 in alleviating ribosome pausing at polyproline motif⁴⁰, were not significantly altered in any of the lines (Fig.
234 S8B). We suspect that the higher ribosome-densities at Proline codons are likely due to lower levels of
235 charged proline tRNAs.

236 237 **Transcriptional and translational changes of frequently deleted genes**

238 Large deletions are among the most frequent class of mutations in the LTEE^{11,12} and several gene
239 deletions are shared across multiple evolved lineages (Fig. 5A). For example, the *rbs* operon is partially or
240 entirely deleted in every evolved line, making them unable to catabolize ribose. This loss of *rbs* operon leads
241 to increased fitness relative to the ancestor⁴¹. We also find that genes deleted entirely in at least four lines
242 had lower expression in the ancestor (Fig. 5B). While the fitness benefit of specific deletions such as *rbs*
243 operon has been experimentally validated, it is more challenging to systematically assess the effects of
244 deletions in only some of the lines. This is especially true of the large deletions that encompass multiple genes
245 of unrelated functions. Since downregulation and deletions of genes have similar functional effects (that is,
246 removal of the gene product), we hypothesized that frequently deleted genes would be typically
247 downregulated in lines where the gene was still present. Surprisingly, we find no enrichment in the
248 downregulation of genes deleted in at least four lines (Fig. 5C). One reason for this lack of enrichment might
249 be the mechanism by which most genes are deleted in LTEE. Deletions in LTEE are typically mediated by
250 insertion-elements, spanning multiple kilobases and encompassing multiple genes (Fig. 5D). On average, 17
251 genes were lost per deletion event. Our results suggest that while deletions of a few genes within these large
252 deletions might be under selection, most of other deletions are simply genetic hitchhikers.
253



254
255 **Figure 5: A.** The frequency with which a gene was deleted entirely across the lines. **B.** Frequently deleted
256 genes have lower expression levels in the ancestors. The distributions of ancestral TPMs of genes were
257 deleted entirely in at least four lines (red) or were never deleted in any of the lines (grey). P-values based on
258 a t-test. **C.** Frequently deleted genes are not typically downregulated in lines where they are present. Heatmap

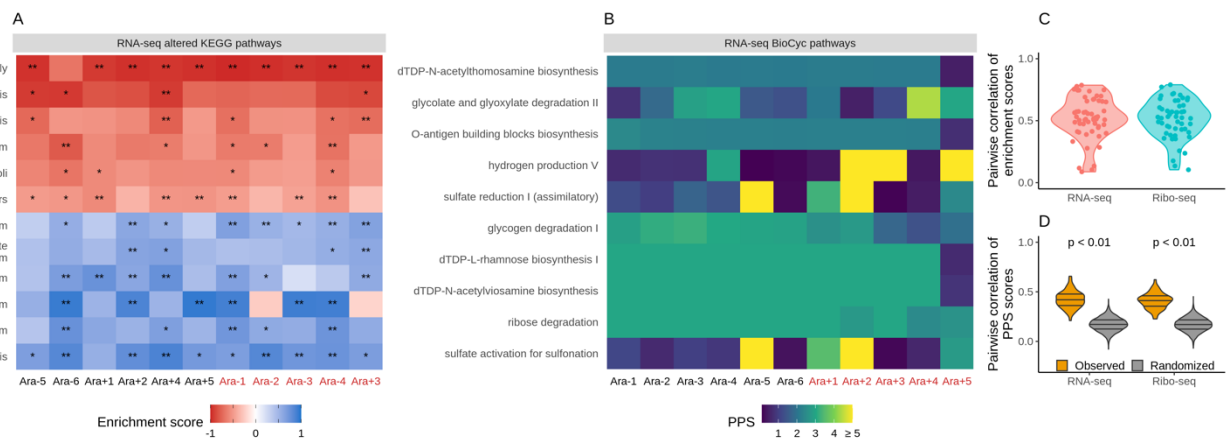
259 represents RNA-seq fold-changes of all genes deleted in at least four lines. Genes are ordered from left to
 260 right in order of increasing mean fold-change across evolved lines. Gray bars represent gene deletions. The
 261 histogram above the heatmap indicates the frequency of deletion of corresponding genes in the heatmap. **D.**
 262 Number of genes deleted per large deletion in LTEE across all 12 lines. The dashed line indicates the average
 263 number of genes deleted per deletion (~17).
 264

265 Functional characterization of differentially expressed genes

266 To identify functional categories and pathways that are altered as a result of expression changes in
 267 each line, we looked for enrichment in KEGG pathways⁴², gene ontology terms⁴³, and pathway perturbation
 268 scores (PPS) from the BioCyc collection of databases⁴⁴ (Fig. S10, Table S13, see methods for details on
 269 each). For these analyses, we considered deleted and pseudogenized genes as being downregulated.
 270

271 Though many categories were altered across the lines in the KEGG analysis (see Table S11 for
 272 complete results), we chose to focus on those that were significantly altered (FDR ≤ 0.05) in at least four lines.
 273 We find a high degree of parallelism between the evolved lines for KEGG pathways that are significantly
 274 altered based on RNA-seq datasets (Fig. 6A, C; see Fig. S9A for Ribo-seq scores). Consistent with earlier
 275 microarray experiments, we find that the flagellar assembly genes are significantly downregulated¹⁶ in 10 out
 276 of 11 evolved lines. In addition, because the evolved lines are growing in a stable environment over
 277 evolutionary timescales, it stands to reason that genes involved in responding to stress and environmental
 278 changes will be downregulated. As expected, we find that genes associated with biofilm formation, two-
 279 component signaling pathways, and ABC transporters are all downregulated across most lines. Furthermore,
 280 we find that selection for faster growth in LTEE has led to significant increases in expression levels of genes
 281 involved in amino acid biosynthesis and sugar metabolism across all lines. These findings are also mirrored
 282 when we use Ribo-seq data for the KEGG analysis (Fig. S9A).
 283

283



284

285 Figure 6: **A.** Parallel changes in functional categories. KEGG enrichment scores from the RNAseq data.
 286 Enrichment score represents the degree to which a pathway was up (positive) or downregulated (negative).
 287 The functional categories are ordered by increasing the mean enrichment score across the lines. **B.** Pathway
 288 perturbation score (PPS) is calculated from RNA-seq fold changes. Higher PPS indicates larger degrees of
 289 alteration but does not indicate directionality. **C.** Pairwise correlations of KEGG enrichment scores for all
 290 pathways that were significantly altered in at least one line. **D.** Pairwise correlations of PPS scores. PPS
 291 scores for the randomized set was calculated by randomizing the fold-changes within each line.
 292

293 While KEGG pathway analysis encompasses molecular interactions and reaction networks, we
 294 wondered which specific metabolic pathways were altered across all lines and which ones remained mostly
 295 unchanged over 50,000 generations. Because *E. coli* REL606 is annotated in the Biocyc collection of
 296 databases, we used their metabolic mapping tool to score pathway alterations with a pathway perturbation

297 score (PPS) in each of the evolved lines (see methods for a detailed explanation of the scoring). Similar to
 298 the KEGG pathway analysis, we find a high degree of parallelism, even at the level of specific metabolic
 299 pathways (Fig. 6B, D). Interestingly, 4 out of 5 most altered pathways are involved in lipopolysaccharides
 300 (LPS) biosynthesis, a major component of Gram-negative bacteria's outer membrane. This indicates that in
 301 addition to changes in cell size and shape, the composition of the evolved lines' outer membrane has
 302 significantly changed. Nonetheless, there is a core set of unaltered pathways, even in clones with a mutator
 303 phenotype. Pathways with low PPS scores, indicating low levels of alteration included D-serine degradation
 304 (mean RNAseq PPS = 0.12, sd = 0.13), pseudouridine degradation (mean RNAseq PPS = 0.11, sd = 0.06),
 305 and others (see Table S12 for complete PPS scores). These may represent pathways with activity levels that
 306 cannot be altered or whose alteration provides little to no fitness benefit.

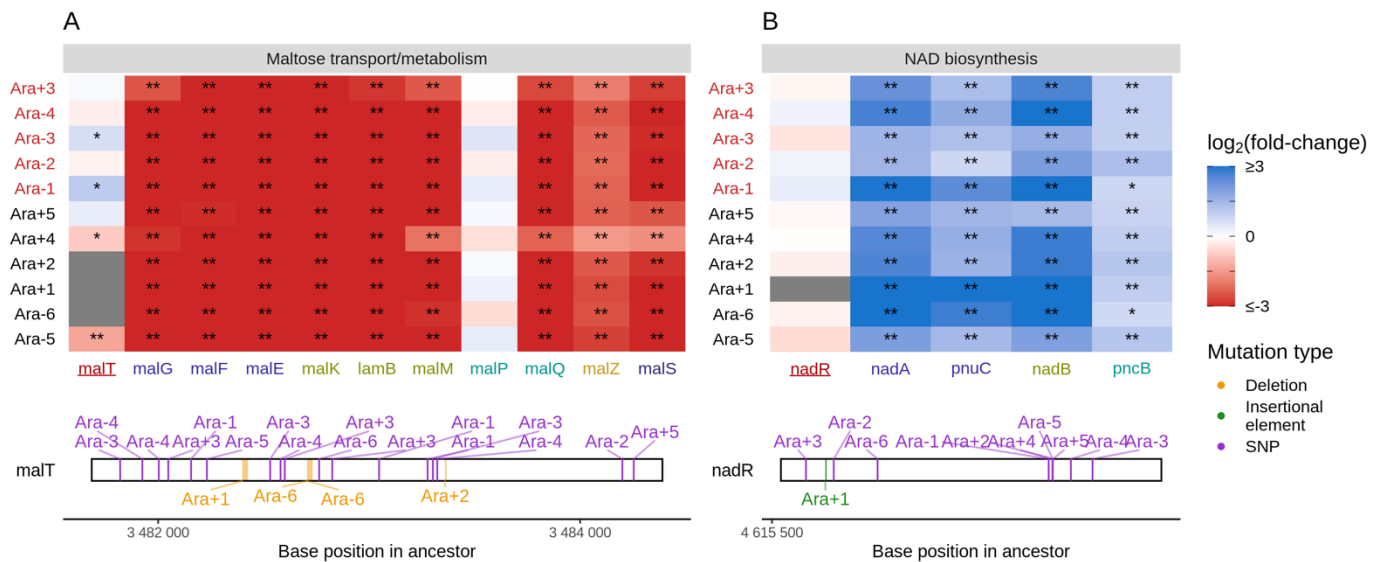
307

308 Mutations to transcriptional regulators explain many parallel expression changes

309

310 Given the high degree of parallelism in evolved lines at the gene expression level, we wondered
 311 whether some of these patterns could be explained by a parallel set of mutations at the genetic level. Because
 312 KEGG, PPS, and GO analyses all identified metabolism and catabolism of various sugars to be significantly
 313 altered, we started by looking at mutations to genes involved in these categories. Previous work has shown
 314 that depending on the generation sampled, evolved clones grow poorly (20,000th generation) or not at all
 315 (50,000th generation) on maltose⁴⁵. Because maltose is absent from the growth media in the LTEE,
 316 maintenance of these transporters is likely unnecessary⁴⁶. Additionally, at 20,000 generations, the
 317 transcriptional activator of the operon responsible for maltose metabolism, *malT*, was the frequent target of
 318 mutations that reduced its ability to act as a transcriptional factor, and introduction of *malT* mutations in the
 319 ancestor had a fitness benefit⁴⁶. In *E. coli*, MalT regulates the transcription of several operons - *malEFG*
 320 (maltose ABC transporter), *malK-lamB-malM* (MalK, part of maltose ABC transporter; LamB, maltose
 321 transporter; MalM, conserved gene of unknown function, MalPQ (two enzymes involved in maltose
 322 metabolism), and the genes *malZ* (maltodextrin glucosidase) and *malS* (an α -amylase). We find that each of
 323 these operons was consistently and significantly downregulated across all lines (Fig. 6E). Changes to the
 324

324



325

326 Figure 7. Mutations in transcriptional regulators lead to parallel changes in gene expression. RNA-seq fold-
 327 changes for genes belonging to **A.** maltose-transport/metabolism and **B.** NAD biosynthesis. Gene names in
 328 each category are colored based on their operon membership. Mutations in transcriptional activator *malT*
 329 decrease expression of its downstream genes/operons. Mutations in transcriptional repressor *nadR* increase
 330 expression of its downstream genes/operons. Asterisks indicate statistical significance of fold-changes, ** q

331 ≤ 0.01 , * $q \leq 0.05$. Grey panels in the heatmap indicate gene deletion. Lower panels show the type and
332 location of mutations in each transcription factor.

333

334 In the LTEE, *NadR*, a transcriptional repressor of genes involved in NAD biosynthesis, is known to be
335 frequently mutated, with many mutations occurring in its DNA binding domain^{48,49}. In fact, all evolved clones
336 used in this study are known to have some mutation in *nadR*¹². Given the high frequency of parallel inactivating
337 mutations in *nadR*, it is likely that these mutations are adaptive as they might increase intracellular NAD
338 concentrations leading to faster growth^{48,49}. We find that genes directly under the regulation of *nadR* -- the
339 *nadAP* operon consisting of *nadA* (quinolinate synthase) and *pnuC* (nicotinamide riboside transporter), and
340 genes -- *nadB* (L-aspartate oxidase) and *pncB* (nicotinate phosphoribosyltransferase), were significantly
341 upregulated in all lines. We also found enrichment of NAD pathways based on KEGG, GO (GO:0019674,
342 GO:0009435), and PPS analysis. Interestingly, four non-operonic genes *nadCDEK*, which play various NAD
343 biosynthesis roles but are not regulated by *nadR*, were largely unaltered (*nadE* was statistically significantly
344 upregulated in 4 lines, DESeq2 $q \leq 0.01$, Table S7). Concordantly, their transcriptional regulator, *nac*, is rarely
345 mutated. This may suggest some sort of specificity to how NAD levels may be increased.

346

347 In addition to linking the effects of specific mutations on gene expression changes in maltose and NAD
348 regulation, we have also identified mutations that likely change the expression of genes involved in arginine
349 biosynthesis, glyoxylate bypass system, and copper balance (Fig. S11, see supplementary methods).
350 However, there also exist several functionally-related sets of genes, such as flagellar assembly, sulfur
351 homeostasis, and biosynthesis of one-carbon compounds – that have parallel changes in expression levels
352 without any obvious sets of parallel mutations linking these changes (Fig. S11). The data generated in this
353 study will likely prove to be a rich resource for understanding the metabolic changes that occur over long
354 periods of evolution in a simple environment such as in the LTEE, thereby adding a rich new dimension to
355 the well-studied mutational changes and gene-expression changes described here.

356

357 Discussion

358 Adaptation to novel environments often takes unique mutational paths even when the tempo and mode
359 of adaptation are similar across populations^{8,12,50–53}. This is due, in part, to the fact that most genetic networks
360 are highly redundant and that many mutations have pleiotropic effects. To bridge the gap between parallel
361 fitness gains in a system with mostly unique genetic changes, we wanted to study gene expression – a main
362 link between genotype and fitness. To that end, we generated RNA-seq and Ribo-seq datasets for individual
363 clones from the ancestral strains and 11 populations evolving under a constant environment for 50,000
364 generations in the *E. coli* long-term evolution experiment. Using these datasets, we have characterized the
365 landscape of gene expression changes and elucidated several key features of the molecular mechanisms
366 involved. First, we show that the evolved lines in the LTEE have remarkably parallel exponential phase
367 expression profiles after 50,000 generations. Second, these changes primarily occurred at the transcriptional
368 level, with translational changes following suit. Nonetheless, we identified signatures of global increases in
369 translation termination rates. Third, transcriptional regulators of genes that were mutated in multiple lines had
370 similar functional effects on their downstream targets across all lines. This indicates a strong penetrance of
371 mutational effects to the phenotypic level even when half of the evolved lines had a hypermutable phenotype.
372 Fourth, we show how functional consequences of mutations are consistent with adaptation in a constant
373 environment -- genes involved in central metabolism and amino-acid biosynthesis are consistently
374 upregulated, and genes involved in sensing environmental changes and stress responses are downregulated.

375

376 Relating gene expression changes to specific mutations in LTEE is far from perfect. For many genes
377 that are functionally related and show parallel changes in gene expression, such as the ones involved in
378 flagellar assembly and sulfur homeostasis, we find few mutations around their coding sequences or
379 sequences of their known transcriptional regulators. This might be due to two factors: (i) a lack of complete

380 knowledge of gene regulatory networks underlying these functions, and (ii) parallel epigenetic changes such
381 as changes in DNA supercoiling heterogeneities, affecting promoter activity⁵⁴. Indeed, changes to DNA
382 superhelicity occur in multiple LTEE lines⁵⁵. Another key challenge in attributing expression changes to
383 mutations is that half of the evolved lines in LTEE have a hypermutable phenotype. These genotypes have
384 ~100-fold higher mutational load than their non-mutator counterparts. It is remarkable that despite a higher
385 mutational burden, expression patterns between mutator and non-mutator lines are highly correlated,
386 suggesting that the bulk of the additional mutations are indeed passenger mutations¹³. While our current study
387 has focused on expression patterns in the exponential phase, populations in the LTEE spend most of their
388 time before serial transfer in the stationary phase. However, it remains unclear if we would observe a similar
389 level of parallelism in the stationary growth phase or how similar the expression profiles might be across
390 distinct growth phases. Taking a multi-omics approach, like the one presented above, will provide critical
391 insights into the tradeoff between expression patterns across phases. Lab evolution experiments combined
392 with high-throughput multi-level sequencing approaches offer a rich resource for studying the molecular
393 mechanisms underlying complex adaptations and provide insights into the repeatability of evolution.

394

395 **ACKNOWLEDGEMENTS**

396 We thank Richard Lenski for generously providing clones from ancestral and 50,000 generations of the LTEE.
397 P.S. is supported by NIH/NIGMS grant R35 GM124976, NSF DBI 1936046, subcontracts from NIH/NIDDK
398 R01 DK056645, R01 DK109714, and R01 DK124369, as well as start-up funds from the Human Genetics
399 Institute of New Jersey at Rutgers University. S.S.Y is supported by start-up funds from the Waksman Institute
400 and Rutgers University

401

402 **AUTHOR CONTRIBUTIONS**

403 P.S. conceived the study and designed the experiments; J.S.F., S.L, and S.S.Y. conducted experiments;
404 J.S.F., S.S.Y., and P.S. analyzed data. J.S.F. and P.S. wrote the manuscript with input from S.L. and S.S.Y.

405

406 **METHODS**

407

408 **Bacterial cell culture, recovery, and lysis**

409 Richard Lenski generously provided clones from LTEE. Specifically, the following clones were used:
410 Ara-1, 11330; Ara+1, 11392; Ara-2, 11333; Ara+2, 11342; Ara-3, 11364; Ara+3, 11345; Ara-4, 11336; Ara+4,
411 11348; Ara-5, 11339; Ara+5, 11367; Ara-6, 11389; Ara+6, 11370. Clones were grown in DM25 medium
412 (HiMedia M390) supplemented with 4 g/L glucose. Each culture was grown in 50 mL in a shaking incubator
413 at 37 C at 125 rpm until an OD600 of 0.4-0.5 was reached. Cells were recovered via vacuum filtration and
414 immediately frozen in liquid nitrogen (LN₂). Frozen pellets were stored at -80 C until lysis. For lysis, a mortar
415 and pestle were chilled to cryogenic temperatures with LN₂. The pellet was ground to a powder while
416 submerged in LN₂. Once pulverized, 650 uL of lysis buffer was added to each sample and ground further.
417 Lysis buffer contained the following: 20 mM Tris pH 8, 10 mM MgCl₂, 100 mM NH₄Cl, 5 mM CaCl₂, 1 mM
418 chloramphenicol, 0.1% v/v sodium deoxycholate, 0.4% v/v Triton X-100, 100 U/mL DNase I, 1 uL/mL
419 SUPERase-In (Thermo Fisher Scientific AM2694). The frozen lysate was allowed to thaw until liquid, then
420 incubated for 10 min on ice to allow complete lysis. Afterward, the lysate was centrifuged at 20,000g for 10
421 minutes at 4 C, and the supernatant recovered and transferred to a new tube. Each sample was split into two
422 for RNA-seq and Ribo-seq libraries.

423

424 **RNA-seq library preparation**

425 Lysate destined for RNA-seq libraries was subjected to total RNA extraction using the Trizol method
426 (Thermo Fisher Scientific 15596026) as per the manufacturer's instructions. RNA was quantified using UV
427 spectrophotometry. We used the ERCC RNA Spike-In Mix (Thermo Fisher Scientific 4456740) in library
428 preparation. For RNA-seq libraries, 3 uL of a 1:100 dilution of the set 1 oligos was added to the first replicate

429 and 4 uL to the second replicate. The spike-ins were added directly to the lysate destined for RNA-seq before
430 Trizol based RNA extraction. 2 ug of RNA with ERCC controls were subjected to fragmentation in a buffer
431 containing final concentrations of 1 mM EDTA, 6 mM Na₂CO₃, and 44 mM NaHCO₃ in a 10 uL reaction volume
432 for 15 minutes at 95 C. 5 uL of loading buffer (final concentrations of 32% v/v formamide, 3.3 mM EDTA, 100
433 ug/mL bromophenol blue) was added to each sample, and the resulting 15 uL mixture was separated by gel
434 electrophoresis with a 15% polyacrylamide TBE-urea gel (Invitrogen EC68852BOX) at 200 V for 30 minutes.
435 Gels were stained for 3 minutes with SYBR Gold (Thermo Fisher Scientific S11494), and the region
436 corresponding to the 18-50 nucleotide sized fragments excised. We excised this region so that we would have
437 similarly sized fragments for both RNA-seq and Ribo-seq libraries. RNA was recovered from the extracted
438 fragments by adding 400 uL a buffer containing 300 mM sodium acetate, 1 mM EDTA, and .25% w/v SDS,
439 and freezing the samples on dry ice for 30 minutes. Then, samples were incubated overnight on a shaker at
440 22 C. 1.5 uL of GlycoBlue (Thermo Fisher Scientific AM9515) was added as a co-precipitant, followed by 500
441 uL of 100% isopropanol. The samples were chilled on ice for 1 hour then centrifuged for 30 minutes at 20,000g
442 at 4 C. The supernatant was removed, and the pellet was allowed to air dry for 10 minutes. The pellet was
443 resuspended in 5 uL of water, and 1 uL was used to check RNA concentration via UV spectrophotometry.
444

445 **Ribo-seq library preparation**

446 Lysate destined for Ribo-seq was incubated with 1500 units of micrococcal nuclease (Roche
447 10107921001) and 6 uL of SUPERase-In at 25 C for 1 hour and shaken at 1400 rpm. 2 uL of .5 M EGTA pH
448 8 was added to quench the reaction, which was then placed on ice. The reaction was centrifuged over a
449 900uL sucrose cushion (final concentrations of 20 mM Tris pH 8, 10 mM MgCl₂, 100 mM NH₄Cl, 1 mM
450 chloramphenicol, 2 mM DTT, .9 M sucrose, 20 U/mL SUPERase-In) using a Beckman Coulter TLA100 rotor
451 at 70,000 rpm at 4 C for 2 hours in a 13 mm x 51 mm polycarbonate ultracentrifuge tube (Beckman Coulter
452 349622). The sucrose solution was removed from the tube, and the pellet resuspended in 300 uL of Trizol,
453 mixed by vortexing, and RNA was extracted according to the manufacturer's protocol. Samples were then
454 separated by gel electrophoresis and purified in the same manner as for RNA-seq.
455

456 **Unified library preparation**

457 Once fragments were obtained from RNA-seq and Ribo-seq samples, they could be subject to a
458 unified library preparation protocol. In total, 8 pooled libraries were prepared, with each library consisting of a
459 single replicate of 6 Ara⁺ or 6 Ara⁻ clones of one sequencing type. For example, one library would consist of
460 replicate 1 of Ara⁻ 1-6 for RNA-seq, and another would consist of the second replicate. The final library
461 structure was 5' adapter - 4 random bases - insert - 5 random bases - sample barcode - 3' adapter. The
462 randomized bases function as UMIs for deduplication.
463

464 3' dephosphorylation was performed by incubating fragments with 10 U/uL T4 Polynucleotide Kinase
465 (New England Biolabs M0201S) in the supplied buffer (NEB B0201S) along with SUPERase-In for 1 hour at
466 37 C in a reaction volume of 5 uL.
467

468 Linker ligation took place by adding the following reagents to the above reaction to the indicated final
469 concentrations: 17% w/v PEG-8000, 200 U/uL of T4 RNA Ligase 2 (NEB M0351S), 1X T4 RNA Ligase
470 Reaction Buffer (NEB B0216L), and 20 uM pre-adenylated linkers. The reaction volume totaled 10 uL, and
471 was incubated for 3 hours at 22 C. Afterwards, 10 U/uL of 5' deadenylase (NEB M0331S), 10 U/uL Rec J
472 exonuclease (Epicentre RJ411250), and the included buffer were added and incubated at 30 C for 45 minutes.
473

474 RNA was purified using a Zymo Research Oligo Clean & Concentrator Kit (Zymo, D4060), and then
475 rRNA depleted using the Illumina Ribo-Zero rRNA Depletion Kit for bacteria, both steps being performed
476 according to the manufacturer's instructions.
477

478 5' phosphorylation was performed by mixing 6 uL of rRNA depleted RNA with 1 uL of 10X PNK buffer
479 (NEB B0201S), 1 uL of PNK enzyme (NEB M0236S), and 2 uL of 1mM ATP to total 10 uL and incubated at
480 37 C for 30 minutes followed by inactivation by heating to 65 C for 20 minutes.

481
482 Hybridization with the reverse transcription primers was performed by adding 1 uL of SR RT Primer
483 (NEB E7333A) to the above reaction and incubating at 75 C for 5 minutes, 37 C for 15 minutes, and 25 C for
484 15 minutes.

485
486 5' adapter ligation was performed by adding 3 uL of 10uM 5' adaptor (which was previously denatured
487 by heating to 70 C for 2 minutes and placed on ice, NEB E7330L), 2 uL of 10X T4 RNA ligation buffer (NEB
488 B0216L), 2 uL of 10mM ATP, 2 uL of T4 RNA ligase I (NEB M0204S) totaling 20 uL and incubated for 1 hour
489 at 30 C.

490
491 Reverse transcription was performed by adding the following to the above reaction: 8 uL of 5x first
492 strand buffer (NEB E7330L), 2 uL of 10mM dNTPs (each), 4 uL of 10X DTT (Invitrogen *something*), 2 uL of
493 SUPERase-In, 2uL of SuperScript II (NEB M0368L), and 2 uL of water, totaling 40 uL and incubated at 50 C
494 for 1 hour then inactivated by heating to 70 C for 15 minutes.

495
496 PCR amplification of the above reaction was performed by taking 150 ng of cDNA template and adding
497 10 uL 5X Phusion HF buffer (Thermo Fisher Scientific F518L), 1uL 10 mM dNTPs (each), 1.25 uL 10uM SR
498 primer (from NEB E7330L), 1.25 uL 10uM index 3 primers, .5 uL of Phusion polymerase (NEB M0530S), and
499 enough to water to total the reaction volume at 50 uL. This was cycled as follows in a thermocycler: 30 sec at
500 90 C; 14 cycles of 15 sec at 94 C, 30 sec at 62 C, 15 sec at 70 C; 5 min at 70 C.

501
502 PCR products were separated by gel electrophoresis on a 6% polyacrylamide gel at 120 V for 45
503 minutes. The region corresponding to the expected product size was excised and purified from the gel by
504 soaking the resected pieces in 250 ul DNA gel elution buffer (NEB E7324A) at 22 C and 200 rpm overnight
505 on a rotator and transferring the solution to a gel filtration spin column (Corning 8160) and centrifuging for 2
506 minutes at 16,000g. 1.5 uL of GlycoBlue, 25 uL of 3M sodium acetate pH 5.5, and 750 uL of 100% ethanol
507 were added, and the solution was held on ice for 2 hours, then centrifuged at 20,000g at 4 C for 30 minutes.
508 The supernatant was removed, and the pellet washed with 75 % ethanol and again centrifuged at 20,000g at
509 4 C for 5 minutes. The pellet was allowed to air dry and resuspended with 11 uL of water. 1 uL was used to
510 check concentration via UV spectrophotometry. The completed libraries were sequenced on Illumina NextSeq
511 in 75 bp single-end mode.

512 **ERCC spike-in controls and modeling**

513 ERCC RNA Spike-In Mix (Thermo Fisher Scientific 4456740) was used in library preparation. For
514 RNA-seq libraries, 3 uL of a 1:100 dilution of the set 1 oligos was added to the first replicate and 4 uL to the
515 second replicate. The spike-ins were added directly to the lysate destined for RNA-seq before Trizol based
516 RNA extraction. The file "absolute_counts.Rmd" contains the code for the linear modeling using the ERCC
517 data.

518 **CFU determination**

519 Before recovery, 1mL of culture was extracted for CFU determination. LB agar plates were used for
520 colony growth. We performed a dilution series of that 1mL culture from 1:10 to 1:1e6 in increments of 10.
521 100uL of each dilution was spread on a plate and incubated overnight at 37C. We determined CFU counts
522 manually from the most appropriate dilution for each culture, usually between 1:1e3 and 1:1e6 dilutions.

523 **Optical microscopy**

527 (i) Media and growth conditions

528 Liquid cultures were grown at 37 °C with aeration, unless otherwise indicated, in DM25 liquid medium (Davis
529 minimal broth supplemented with glucose at a concentration of 25 mg per L¹⁰).

530

531 (ii) Microscopy

532 Prior to each experiment, clones were grown in liquid cultures in DM25 medium overnight at 37 °C with
533 aeration. OD₆₀₀ of the cultures were ~0.1–0.3. Microscope slides were prepared with 1% agarose pads, and
534 cells were imaged by microscopy. Phase-contrast microscopy was performed using an Olympus IX81
535 microscope with a 100-W mercury lamp and 100× NA 1.35 objective lens. 16-bit images were acquired with
536 a SensiCam QE cooled charge-coupled device camera (Cooke Corp.) and IPLab version 3.7 software
537 (Scanalytics) with 2 × 2 binning. Average cell lengths were determined from phase contrast images using
538 ImageJ⁵⁶ and the MicrobeJ plugin⁵⁷.

539

540 **Sequencing data processing**

541 Sequencing data are deposited here - <https://www.ncbi.nlm.nih.gov/geo/query/acc.cgi?acc=GSE164308>.
542 Code for all data processing and subsequent analysis can be found in a series of R markdown documents
543 here – (<https://github.com/shahlab/LTEE-gene-expression>). The file titled "data_processing.Rmd" contains
544 the code for processing of the raw sequencing data. We processed 8 raw data files. We used Cutadapt⁵⁸ to
545 remove adapters and retained only reads that had successful trimming. We then used the dedupe.sh script
546 from the BBtools suite to remove PCR duplicates. Files were demultiplexed using the FASTX-Toolkit
547 barcode splitter script. After demultiplexing, barcodes and the randomized adapters were removed using
548 cutadapt. The 4 nucleotide UMIs were removed from the 5' end of a read and 10 nucleotides from the 3' end
549 (5 UMI + 5 barcode). Only reads longer than 24 nucleotides after trimming were retained.

550

551 **Alignment**

552

553 **Differential expression**

554 Code for this section can be found in the file titled "DEseq2.Rmd". We used DEseq2³⁰ with the
555 "apeglm" normalization⁵⁹ for differential expression. In estimating fold-changes, we compared the 4 replicates
556 of the ancestors (2 each from ancestors of Ara+ and Ara-) to 2 replicates of each of the evolved lines. Because
557 some genes in some lines contained indels or were deleted entirely, some transcripts were missing from the
558 transcriptome fastas used to create indices for alignment. We added these genes back to Kallisto's counts
559 with estimated counts of 0 and assigned them fold-changes of NA. Count matrices containing identical
560 complements of transcripts were used in the differential expression analysis for each line, such that all evolved
561 lines had the same complement of genes as the ancestors.

562

563 **Change in ribosomal density analysis**

564 We used Riborex³⁴ to analyze changes in ribosomal density. The same count matrices used for
565 DEseq2 were used here, and comparisons were made in the same manner of 4 ancestral samples (2 lines,
566 2 replicate each) to 2 evolved clones (1 line, 2 replicates). The code for this section can be found in the file
567 "riborex.Rmd"

568

569 **Codon specific positioning of Ribo-seq data**

570 Code for this section can be found in the file "codon_specific_densities.Rmd". We used hisat2⁶⁰ to
571 align our Ribo-seq data to each clone's unique genome and marked the A site position of a read using a fixed
572 offset of 37nt from the 3' end of a read. It has been shown that mapping bacterial Ribo-seq reads by their 3'
573 ends is more accurate than 5' mapping⁶¹. We then calculated genome-wide ribosome density at each codon
574 using only genes that had at least 100 reads. The distributions of read counts per gene can be seen in figure
575 S1C. Only bacterial protein-coding genes (not tRNA or insertional element genes) were considered. To

576 calculate ribosome densities on a codon for a gene, the number of reads mapping to a codon was normalized
577 to the total number of reads mapping to that gene in a replicate and line-specific manner. Genome-wide codon
578 density is calculated by taking genes with at least 100 reads mapping to them and taking the average number
579 of normalized reads mapping to each codon across that set of genes as the genome-wide codon density.

580

581 **Functional analysis**

582 We used three different functional analysis methods – GO (using the R package topGO), KEGG (using
583 the R package clusterProfiler⁶², and PPS⁴⁴. The code for each of these analyses can be found in the Rmd
584 files named "go.Rmd", "kegg_analysis.Rmd", and "manual_PPS.Rmd," respectively. We used a manual
585 implementation of the Biocyc PPS score because the website was not capable of high throughput analysis.
586 Briefly, each pathway is composed of at least one reaction, and each reaction is completed by at least one
587 enzyme. First, a reaction perturbation score is calculated for each reaction in a pathway. It is defined as the
588 absolute value of the largest fold-change of an enzyme associated with that reaction. To calculate PPS, for a
589 pathway having N reactions, $PPS = \sqrt{(\sum RPS^2) / N}$.

590

591 **SUPPLEMENTAL ANALYSIS**

592

593 **Cell size and filamentation**

594 Evolved lines form filaments more frequently and form longer filaments compared to the ancestor.
595 This is supported by the fact that all evolved lines except Ara+1 had significantly longer cells compared to the
596 ancestor (Welch's t-test, $p < .0001$ for all lines) (Fig. S2A). Additionally, volume and aspect ratio are positively
597 correlated in all lines ($0.53 \leq R \leq 0.94$). Length and volume was positively correlated ($0.76 \leq R \leq 0.95$), but
598 width and volume showed a low correlation ($0.12 \leq R \leq 0.45$) (Fig. S2C). Taken together, increases in the
599 volume to large values are due to increases in one dimension, length, suggesting increased filamentation.
600 We designated cells that are greater than three times the median volume of a given line as filaments. Even
601 after removing filaments from the comparisons, each evolved line was still larger in volume than the ancestor
602 (Fig. S2B). Removal of filaments did not alter the relationship between the median volume and RNAs per
603 CFU (Fig. S2D).

604

605 **CFU counts**

606 One caveat to the relationship between CFU counts and RNA abundance is that the CFU counts may
607 be misleading, especially in light of the increased filamentation suggested by our microscopy data. Because
608 a single chain of bacteria composed of multiple cells could be the source of a single colony, the CFUs may
609 be an underestimate of the number of cells that had gone into the preparation of each of the evolved lines
610 libraries. If this was the case, it might contribute to the observed results.

611

612 **GO analysis**

613 We also performed GO searches in all three ontologies, Cellular compartment (CC), Biological process
614 (BP), and Molecular function (MF). The top 5 up and downregulated terms for each ontology can be seen in
615 Fig. S11, and the complete results can be found in Supplementary Table S13. These searches found results
616 similar to the KEGG and PPS results. For example, terms related to the flagellar apparatus (BP, GO:0044780,
617 GO:0044781, GO:0071978, GO:0097588, GO:0071973, GO:0001539; CC, GO:0009288 GO:0009424,
618 GO:0044461), polysaccharide transport (BP, GO:0015774, GO:0033037), specifically, maltodextrin transport
619 (BP, GO:0042956), arginine biosynthesis (BP: GO:0006526), and others reach statistical significance
620 (Fisher's exact test, $p \leq 0.05$) in many of the lines. Other terms related to iron were also found to be enriched
621 and many genes related to iron transport or incorporation into organic molecules were found to have
622 significant fold-changes in the DESeq2 results (data not shown, see table S7 for complete DESeq2 results).

623

624 **Analysis of altered pathways**

625 Flagella are used for bacterial motility and allow bacteria to move to new environments by swimming.
626 Previous experiments in the LTEE have shown the downregulation of flagellar apparatus genes in Ara+1 and
627 Ara-1 at 20,000 generations, though the exact source of these downregulations was not determined¹⁶. We
628 find that genes related to the flagellar apparatus are significantly downregulated in 10 of the 11 lines
629 considered here (Fig. S11A). The flgBCDEFGHIJK, flgAMN, and flhABE operons are significantly
630 downregulated in all but Ara-6, where only some of these genes were downregulated. These operons
631 contribute various proteins to the flagellar apparatus and are regulated in part by the transcription factors flhC
632 and flhD, which have complicated regulation dictated by various environmental factors⁶³. flhC and flhD are
633 downregulated in 3 of the evolved lines but mostly unaltered in the others. These genes are rarely mutated in
634 the clones used in this study (Fig. S11A, bottom). The fitness benefits of downregulation to the flagellar
635 apparatus may be multifaceted. The flagellar apparatus is an expensive piece of machinery to produce, and
636 it requires energy to move. Other *E. coli* evolution studies have shown that mutations in flagellar genes are
637 common and provide a fitness advantage⁶⁴. Additionally, the *E. coli* B strain is thought to be non-motile⁶⁵.
638 Taken together, the downregulation of flagella may simply be the removal of an unused system. Surprisingly,
639 the lack of parallel changes in transcriptional regulators flhCD indicates that it is unlikely that transcriptional
640 changes are the primary mode for downregulation of the flagellar protein operons.

641
642 Amino acids are the building blocks for proteins, and translation of new proteins is required for cellular
643 growth. Hence, increased levels of intracellular amino acids would allow faster translation of proteins and
644 faster growth. Terms involving amino acid biosynthesis showed up frequently in all three methods used for
645 functional analysis (KEGG, GO, and PPS). Arginine biosynthesis (KEGG and GO:0006526) was a frequently
646 upregulated category. We find that genes related to arginine biosynthesis were upregulated in 8 out of 11
647 lines (Fig. S11B). These genes are partly controlled by the argR repressor, which represses their transcription
648 when L-arginine is abundant⁶⁶. 5 out of 10 lines had mutations to the argR coding sequence, and other lines
649 had mutations occurring nearby. Interestingly, we find that expression levels of argR remain unchanged in all
650 lines indicating that these mutations may have disabled argR function, causing de-repression of its
651 downstream targets.

652
653 The glyoxylate bypass system allows *E. coli* to utilize acetate as a carbon source, is composed of the
654 aceBAK operon, and regulated by iclR and arcAB⁶⁷. Acetate is a metabolic by-product but can be returned to
655 central carbon metabolism for biosynthetic reactions by this system. Previous studies have shown that
656 mutations in iclR and arcB cause depression of their target genes are beneficial in the LTEE⁶⁸. Consistent
657 with these results, we found that the aceBAK operon was upregulated in 9 of 11 evolved lines (Fig. S11C).

658
659 Copper and silver have antibacterial properties⁶⁹, and bacteria have evolved systems to mitigate
660 toxicity from these elements. The cusCFBA operon, regulated by the cusRS sensor kinase, codes for proteins
661 that transport copper and silver ions out of the cell⁷⁰. Additionally, the cytoplasmic copper chaperone copA,
662 regulated by cueR⁷¹, and cueO (multicopper oxidase⁷²) regulate copper homeostasis in the cell. These genes
663 contained deletions 5 of our clones and were downregulated in 3 of the 6 lines where they remained (Fig.
664 S11D). Overall, 8 of the 11 lines surveyed here had defects in these systems. This suggests that there may
665 be the selection for removal or downregulation of these genes. In contrast to natural environments, the
666 laboratory environment is likely free of copper and silver, rendering these systems dispensable.

667
668 Sulfur is a critical component of many biological molecules, like amino acids, and participates in
669 creating other structures like iron-sulfur cluster proteins. Organic sulfur is transported across the cell
670 membrane by proteins from the cysPUWAM operon, which encodes for a sulfate/thiosulfate importer⁷³, the
671 gsiABCD operon which encodes for a glutathione importer⁷⁴, the tauABCD operon which codes for a taurine
672 importer⁷⁵, and tcyP, the major L-cysteine importer⁷⁶. We found that many of these genes were downregulated
673 in many of the lines (Fig. S11E). The cysB gene positively regulates these genes and was downregulated in

674 most lines. This gene contained few mutations across the lines. The sources of organic sulfur in the medium
675 used in the LTEE are ammonium and magnesium sulfate, for which the *cysPUWAM* operon functions as the
676 importer. The mechanism and reasons for alterations to these operons remain unclear. The amount of organic
677 sulfur in the medium may be sufficient to allow the downregulation of sulfur transport systems without
678 impacting downstream pathways that require sulfur.

679

680 Glycine plays a role in protein construction and can serve as a building block for other metabolic
681 pathways such as one-carbon metabolism or serine synthesis^{67,77}. We found that the *gcvTHP* operon, which
682 encodes for proteins in the glycine cleavage system, were upregulated in 6 of the 11 lines. Increases in the
683 levels of compounds involved in this set of reactions directly may increase the growth rate. Though there are
684 some mutations in and around transcriptional regulators of these genes, their effects are unclear. Whether
685 changes to these genes are due to changes in their transcription factors or other changes, the upregulation
686 of these genes in many lines suggests that it may be beneficial.

687

688

689 **Supplemental tables**

690

691 A description of the supplemental tables:

692

693 Table S1: The file "table_s1_read_counts.csv" contains quantification of read counts per gene based on
694 Kallisto for each sample. Counts in this file were rounded, and new TPMs were calculated based on rounded
695 counts. This file was generated using "data_cleaning.Rmd".

696 Table S2: The file "table_s2_three_nt_periodicity.csv" contains the data needed to show periodicity in the
697 Ribo-seq data. This file was generated using "3nt_periodicity.Rmd".

698 Table S3: The file "table_s3_cell_size.csv" contains cell size data derived from phase-contrast microscopy.

699 Table S4: The file "table_s4_colony_counts.csv" contains information about colony forming units for each of
700 the samples.

701 Table S5: The file "table_s5_ercc_molecules_per_sample.csv" contains information about the use of ERCC
702 controls in each sample and the counts/TPMs of each control in each sample.

703 Table S6: The file "table_s6_mRNAs_per_cfu.csv" shows the absolute counts of mRNAs per CFU for each
704 gene in each sample. This file was generated using "absolute_counts.Rmd".

705 Table S7: The file "table_s7_fold-changes.csv" contains the results of gene-expression fold-changes based
706 on DESeq2 analysis. This file was generated using "DEseq2.Rmd".

707 Table S8: The file "table_s8_mutations.csv" contains data on mutations accumulating in LTEE and was
708 derived from Good et al. 2017 and downloaded from <https://barricklab.org/shiny/LTEE-Ecoli/>.

709 Table S9: The file "table_s9_riborex_results.csv" contains the results of differential ribosome-density analysis
710 using Riborex. This file was generated using "riborex.Rmd".

711 Table S10: The file "table_s10_genome_wide_codon_densities.csv" contains the genome-wide codon-
712 specific ribosome-densities. This file was generated using "codon_specific_densities.Rmd".

713 Table S11: The file "table_s11_kegg_results.csv" shows the results of KEGG enrichment analyses. This file
714 was generated using "kegg_analysis.Rmd".

715 Table S12: The file "table_s12_pps_scores" shows the PPS scores analyses. This file was generated using
716 "manual_PPS.Rmd".

717 Table S13: The file "table_s13_go_results.csv" shows the results of GO enrichment analyses. This file was
718 generated using "go.Rmd".

719 **References**

720

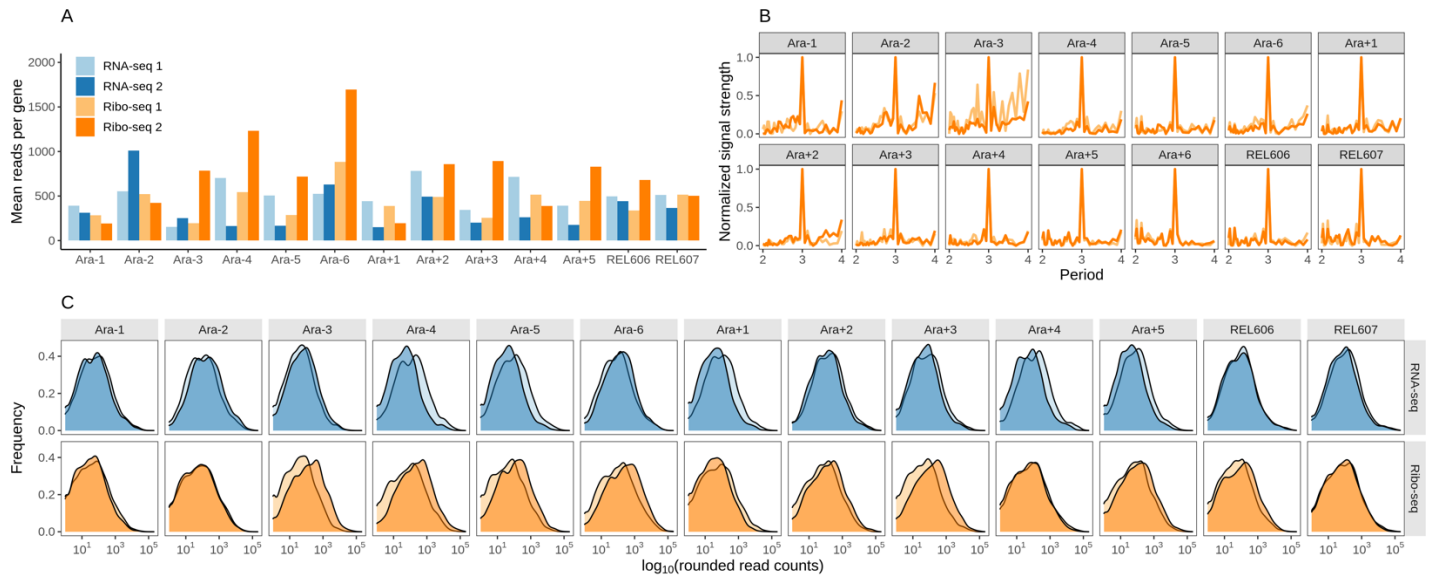
- 721 1. Natarajan, C. *et al.* Epistasis among adaptive mutations in deer mouse hemoglobin. *Science* **340**,
- 722 1324–1327 (2013).
- 723 2. Bridgham, J. T., Ortlund, E. A. & Thornton, J. W. An epistatic ratchet constrains the direction of
- 724 glucocorticoid receptor evolution. *Nature* **461**, 515–519 (2009).
- 725 3. Gong, L. I., Suchard, M. A. & Bloom, J. D. Stability-mediated epistasis constrains the evolution of an
- 726 influenza protein. *Elife* **2**, e00631 (2013).
- 727 4. Lee, J. M. *et al.* Deep mutational scanning of hemagglutinin helps predict evolutionary fates of human
- 728 H3N2 influenza variants. *Proc. Natl. Acad. Sci. U. S. A.* **115**, E8276–E8285 (2018).
- 729 5. Gresham, D. *et al.* The repertoire and dynamics of evolutionary adaptations to controlled nutrient-
- 730 limited environments in yeast. *PLoS Genet.* **4**, e1000303 (2008).
- 731 6. Venkataram, S. *et al.* Development of a Comprehensive Genotype-to-Fitness Map of Adaptation-
- 732 Driving Mutations in Yeast. *Cell* **166**, 1585-1596.e22 (2016).
- 733 7. Lauer, S. *et al.* Single-cell copy number variant detection reveals the dynamics and diversity of
- 734 adaptation. *PLoS Biol.* **16**, e3000069 (2018).
- 735 8. Tenaillon, O. *et al.* The molecular diversity of adaptive convergence. *Science* **335**, 457–461 (2012).
- 736 9. Lieberman, T. D. *et al.* Parallel bacterial evolution within multiple patients identifies candidate
- 737 pathogenicity genes. *Nat. Genet.* **43**, 1275–1280 (2011).
- 738 10. Lenski, R. E., Rose, M. R., Simpson, S. C. & Tadler, S. C. Long-Term Experimental Evolution in
- 739 *Escherichia coli*. I. Adaptation and Divergence During 2,000 Generations. *Am. Nat.* **138**, 1315–1341
- 740 (1991).
- 741 11. Barrick, J. E. *et al.* Genome evolution and adaptation in a long-term experiment with *Escherichia coli*.
- 742 *Nature* **461**, 1243–1247 (2009).
- 743 12. Tenaillon, O. *et al.* Tempo and mode of genome evolution in a 50,000-generation experiment. *Nature*
- 744 **536**, 165–170 (2016).
- 745 13. Good, B. H., McDonald, M. J., Barrick, J. E., Lenski, R. E. & Desai, M. M. The dynamics of molecular
- 746 evolution over 60,000 generations. *Nature* **551**, 45–50 (2017).
- 747 14. Wisser, M. J., Ribeck, N. & Lenski, R. E. Long-Term Dynamics of Adaptation in Asexual Populations.
- 748 *Science* **342**, 1364–1367 (2013).
- 749 15. Blount, Z. D., Barrick, J. E., Davidson, C. J. & Lenski, R. E. Genomic analysis of a key innovation in an
- 750 experimental *Escherichia coli* population. *Nature* **489**, 513–518 (2012).
- 751 16. Cooper, T. F., Rozen, D. E. & Lenski, R. E. Parallel changes in gene expression after 20,000
- 752 generations of evolution in *Escherichia coli*. *Proc. Natl. Acad. Sci. U. S. A.* **100**, 1072–1077 (2003).
- 753 17. Artieri, C. G. & Fraser, H. B. Evolution at two levels of gene expression in yeast. *Genome Res.* **24**,
- 754 411–421 (2014).
- 755 18. McManus, C. J., May, G. E., Spealman, P. & Shteyman, A. Ribosome profiling reveals post-
- 756 transcriptional buffering of divergent gene expression in yeast. *Genome Res.* **24**, 422–430 (2014).
- 757 19. Mongold, J. A. & Lenski, R. E. Experimental rejection of a nonadaptive explanation for increased cell
- 758 size in *Escherichia coli*. *J. Bacteriol.* **178**, 5333–5334 (1996).
- 759 20. Grant, N. A., Magid, A. A., Franklin, J., Dufour, Y. & Lenski, R. E. Changes in Cell Size and Shape
- 760 During 50,000 Generations of Experimental Evolution with *Escherichia coli*. *Cold Spring Harbor*
- 761 *Laboratory* 2020.08.13.250415 (2020) doi:10.1101/2020.08.13.250415.
- 762 21. Ingolia, N. T., Ghaemmaghami, S., Newman, J. R. S. & Weissman, J. S. Genome-wide analysis in vivo
- 763 of translation with nucleotide resolution using ribosome profiling. *Science* **324**, 218–223 (2009).
- 764 22. Lenski, R. E. & Mongold, J. A. Cell size, shape, and fitness in evolving populations of bacteria. in
- 765 *Scaling in biology* 221–235 (Oxford University Press, Inc., 2000).

- 766 23. Schaechter, M., MaalOe, O. & Kjeldgaard, N. O. Dependency on Medium and Temperature of Cell Size
767 and Chemical Composition during Balanced Growth of *Salmonella typhimurium*. *J. Gen. Microbiol.* **19**,
768 592–606 (1958).
- 769 24. Chien, A.-C., Hill, N. S. & Levin, P. A. Cell size control in bacteria. *Curr. Biol.* **22**, R340-9 (2012).
- 770 25. Taheri-Araghi, S. *et al.* Cell-size control and homeostasis in bacteria. *Curr. Biol.* **25**, 385–391 (2015).
- 771 26. Philippe, N., Pelosi, L., Lenski, R. E. & Schneider, D. Evolution of penicillin-binding protein 2
772 concentration and cell shape during a long-term experiment with *Escherichia coli*. *J. Bacteriol.* **191**,
773 909–921 (2009).
- 774 27. Turner, C. B., Wade, B. D., Meyer, J. R., Sommerfeld, B. A. & Lenski, R. E. Evolution of organismal
775 stoichiometry in a long-term experiment with *Escherichia coli*. *R Soc Open Sci* **4**, 170497 (2017).
- 776 28. Padovan-Merhar, O. *et al.* Single mammalian cells compensate for differences in cellular volume and
777 DNA copy number through independent global transcriptional mechanisms. *Mol. Cell* **58**, 339–352
778 (2015).
- 779 29. Baker, S. C. *et al.* The External RNA Controls Consortium: a progress report. *Nat. Methods* **2**, 731–734
780 (2005).
- 781 30. Love, M. I., Huber, W. & Anders, S. Moderated estimation of fold change and dispersion for RNA-seq
782 data with DESeq2. *Genome Biol.* **15**, 550 (2014).
- 783 31. Picard, F. *et al.* Bacterial translational regulations: high diversity between all mRNAs and major role in
784 gene expression. *BMC Genomics* **13**, 528 (2012).
- 785 32. Li, G.-W., Burkhardt, D., Gross, C. & Weissman, J. S. Quantifying absolute protein synthesis rates
786 reveals principles underlying allocation of cellular resources. *Cell* **157**, 624–635 (2014).
- 787 33. Albert, F. W., Muzzey, D., Weissman, J. S. & Kruglyak, L. Genetic influences on translation in yeast.
788 *PLoS Genet.* **10**, e1004692 (2014).
- 789 34. Li, W., Wang, W., Uren, P. J., Penalva, L. O. F. & Smith, A. D. Riborex: fast and flexible identification of
790 differential translation from Ribo-seq data. *Bioinformatics* **33**, 1735–1737 (2017).
- 791 35. Janosi, L., Shimizu, I. & Kaji, A. Ribosome recycling factor (ribosome releasing factor) is essential for
792 bacterial growth. *Proc. Natl. Acad. Sci. U. S. A.* **91**, 4249–4253 (1994).
- 793 36. Kaji, A. *et al.* The fourth step of protein synthesis: disassembly of the posttermination complex is
794 catalyzed by elongation factor G and ribosome recycling factor, a near-perfect mimic of tRNA. *Cold*
795 *Spring Harb. Symp. Quant. Biol.* **66**, 515–529 (2001).
- 796 37. Capecchi, M. R. Polypeptide chain termination in vitro: isolation of a release factor. *Proc. Natl. Acad.*
797 *Sci. U. S. A.* **58**, 1144–1151 (1967).
- 798 38. Capecchi, M. R. & Klein, H. A. Characterization of three proteins involved in polypeptide chain
799 termination. *Cold Spring Harb. Symp. Quant. Biol.* **34**, 469–477 (1969).
- 800 39. Mora, L., Heurgué-Hamard, V., de Zamaroczy, M., Kervestin, S. & Buckingham, R. H. Methylation of
801 bacterial release factors RF1 and RF2 is required for normal translation termination in vivo. *J. Biol.*
802 *Chem.* **282**, 35638–35645 (2007).
- 803 40. Tollerson, R., 2nd, Witzky, A. & Ibbá, M. Elongation factor P is required to maintain proteome
804 homeostasis at high growth rate. *Proc. Natl. Acad. Sci. U. S. A.* **115**, 11072–11077 (2018).
- 805 41. Cooper, V. S., Schneider, D., Blot, M. & Lenski, R. E. Mechanisms causing rapid and parallel losses of
806 ribose catabolism in evolving populations of *Escherichia coli* B. *J. Bacteriol.* **183**, 2834–2841 (2001).
- 807 42. Kanehisa, M. & Goto, S. KEGG: kyoto encyclopedia of genes and genomes. *Nucleic Acids Res.* **28**,
808 27–30 (2000).
- 809 43. Ashburner, M. *et al.* Gene ontology: tool for the unification of biology. The Gene Ontology Consortium.
810 *Nat. Genet.* **25**, 25–29 (2000).
- 811 44. Karp, P. D. *et al.* The BioCyc collection of microbial genomes and metabolic pathways. *Brief. Bioinform.*
812 (2017) doi:10.1093/bib/bbx085.
- 813 45. Leiby, N. & Marx, C. J. Metabolic erosion primarily through mutation accumulation, and not tradeoffs,
814 drives limited evolution of substrate specificity in *Escherichia coli*. *PLoS Biol.* **12**, e1001789 (2014).

- 815 46. Pelosi, L. *et al.* Parallel changes in global protein profiles during long-term experimental evolution in
816 *Escherichia coli*. *Genetics* **173**, 1851–1869 (2006).
- 817 47. Meyer, J. R. *et al.* Parallel changes in host resistance to viral infection during 45,000 generations of
818 relaxed selection. *Evolution* **64**, 3024–3034 (2010).
- 819 48. Ostrowski, E. A., Woods, R. J. & Lenski, R. E. The genetic basis of parallel and divergent phenotypic
820 responses in evolving populations of *Escherichia coli*. *Proc. Biol. Sci.* **275**, 277–284 (2008).
- 821 49. Woods, R., Schneider, D., Winkworth, C. L., Riley, M. A. & Lenski, R. E. Tests of parallel molecular
822 evolution in a long-term experiment with *Escherichia coli*. *Proc. Natl. Acad. Sci. U. S. A.* **103**, 9107–
823 9112 (2006).
- 824 50. Therikildsen, N. O. *et al.* Contrasting genomic shifts underlie parallel phenotypic evolution in response
825 to fishing. *Science* **365**, 487–490 (2019).
- 826 51. Levy, S. F. *et al.* Quantitative evolutionary dynamics using high-resolution lineage tracking. *Nature* **519**,
827 181–186 (2015).
- 828 52. Meyer, J. R. *et al.* Repeatability and contingency in the evolution of a key innovation in phage lambda.
829 *Science* **335**, 428–432 (2012).
- 830 53. Cheng, C. H. Evolution of the diverse antifreeze proteins. *Curr. Opin. Genet. Dev.* **8**, 715–720 (1998).
- 831 54. El Houdaigui, B. *et al.* Bacterial genome architecture shapes global transcriptional regulation by DNA
832 supercoiling. *Nucleic Acids Res.* **47**, 5648–5657 (2019).
- 833 55. Crozat, E. *et al.* Parallel genetic and phenotypic evolution of DNA superhelicity in experimental
834 populations of *Escherichia coli*. *Mol. Biol. Evol.* **27**, 2113–2128 (2010).
- 835 56. Schneider, C. A., Rasband, W. S. & Eliceiri, K. W. NIH Image to ImageJ: 25 years of image analysis.
836 *Nat. Methods* **9**, 671–675 (2012).
- 837 57. Ducret, A., Quardokus, E. M. & Brun, Y. V. MicrobeJ, a tool for high throughput bacterial cell detection
838 and quantitative analysis. *Nat Microbiol* **1**, 16077 (2016).
- 839 58. Martin, M. Cutadapt removes adapter sequences from high-throughput sequencing reads.
840 *EMBnet.journal* **17**, 10–12 (2011).
- 841 59. Zhu, A., Ibrahim, J. G. & Love, M. I. Heavy-tailed prior distributions for sequence count data: removing
842 the noise and preserving large differences. *Bioinformatics* **35**, 2084–2092 (2019).
- 843 60. Kim, D., Paggi, J. M., Park, C., Bennett, C. & Salzberg, S. L. Graph-based genome alignment and
844 genotyping with HISAT2 and HISAT-genotype. *Nat. Biotechnol.* **37**, 907–915 (2019).
- 845 61. Mohammad, F., Green, R. & Buskirk, A. R. A systematically-revised ribosome profiling method for
846 bacteria reveals pauses at single-codon resolution. *Elife* **8**, (2019).
- 847 62. Yu, G., Wang, L.-G., Han, Y. & He, Q.-Y. clusterProfiler: an R package for comparing biological themes
848 among gene clusters. *OMICS* **16**, 284–287 (2012).
- 849 63. Soutourina, O. A. & Bertin, P. N. Regulation cascade of flagellar expression in Gram-negative bacteria.
850 *FEMS Microbiol. Rev.* **27**, 505–523 (2003).
- 851 64. Edwards, R. J., Sockett, R. E. & Brookfield, J. F. Y. A simple method for genome-wide screening for
852 advantageous insertions of mobile DNAs in *Escherichia coli*. *Curr. Biol.* **12**, 863–867 (2002).
- 853 65. Jeong, H. *et al.* Genome sequences of *Escherichia coli* B strains REL606 and BL21(DE3). *J. Mol. Biol.*
854 **394**, 644–652 (2009).
- 855 66. Caldara, M., Charlier, D. & Cunin, R. The arginine regulon of *Escherichia coli*: whole-system
856 transcriptome analysis discovers new genes and provides an integrated view of arginine regulation.
857 *Microbiology* **152**, 3343–3354 (2006).
- 858 67. Okamura-Ikeda, K., Ohmura, Y., Fujiwara, K. & Motokawa, Y. Cloning and nucleotide sequence of the
859 *gcv* operon encoding the *Escherichia coli* glycine-cleavage system. *Eur. J. Biochem.* **216**, 539–548
860 (1993).
- 861 68. Quandt, E. M. *et al.* Fine-tuning citrate synthase flux potentiates and refines metabolic innovation in the
862 Lenski evolution experiment. *Elife* **4**, (2015).

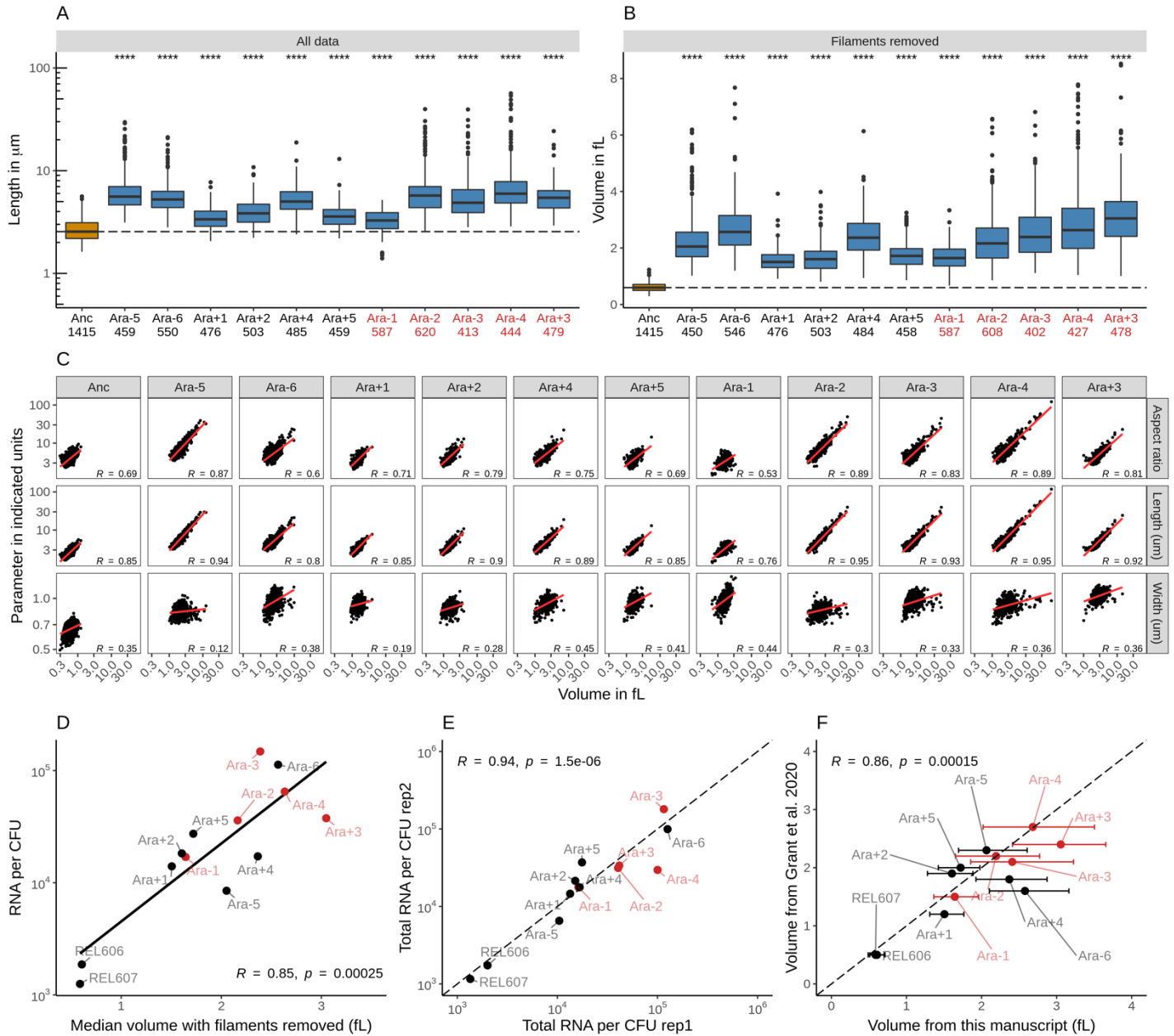
- 863 69. Ingle, A. P., Duran, N. & Rai, M. Bioactivity, mechanism of action, and cytotoxicity of copper-based
864 nanoparticles: a review. *Appl. Microbiol. Biotechnol.* **98**, 1001–1009 (2014).
- 865 70. Nies, D. H. Efflux-mediated heavy metal resistance in prokaryotes. *FEMS Microbiol. Rev.* **27**, 313–339
866 (2003).
- 867 71. Meydan, S. *et al.* Programmed Ribosomal Frameshifting Generates a Copper Transporter and a
868 Copper Chaperone from the Same Gene. *Mol. Cell* **65**, 207–219 (2017).
- 869 72. Grass, G. & Rensing, C. Genes involved in copper homeostasis in *Escherichia coli*. *J. Bacteriol.* **183**,
870 2145–2147 (2001).
- 871 73. Sirko, A., Zatyka, M., Sadowy, E. & Hulanicka, D. Sulfate and thiosulfate transport in *Escherichia coli* K-
872 12: evidence for a functional overlapping of sulfate- and thiosulfate-binding proteins. *J. Bacteriol.* **177**,
873 4134–4136 (1995).
- 874 74. Suzuki, H., Koyanagi, T., Izuka, S., Onishi, A. & Kumagai, H. The *yliA*, -B, -C, and -D genes of
875 *Escherichia coli* K-12 encode a novel glutathione importer with an ATP-binding cassette. *J. Bacteriol.*
876 **187**, 5861–5867 (2005).
- 877 75. Eichhorn, E., van der Ploeg, J. R. & Leisinger, T. Deletion analysis of the *Escherichia coli* taurine and
878 alkanesulfonate transport systems. *J. Bacteriol.* **182**, 2687–2695 (2000).
- 879 76. Chonoles Imlay, K. R., Korshunov, S. & Imlay, J. A. Physiological Roles and Adverse Effects of the
880 Two Cystine Importers of *Escherichia coli*. *J. Bacteriol.* **197**, 3629–3644 (2015).
- 881 77. Wilson, R. L., Steiert, P. S. & Stauffer, G. V. Positive regulation of the *Escherichia coli* glycine cleavage
882 enzyme system. *J. Bacteriol.* **175**, 902–904 (1993).
- 883

884



885

886 Figure S1: Summary of sequencing data. **A**. The average number of reads aligned per protein-coding gene
887 by Kallisto for each sample. The color scheme remains the same for the other panels. **B**. The periodicity of
888 the ribo-seq datasets is determined using a fast Fourier transform (see methods). **C**. Distributions of reads
889 per protein-coding gene in each sample.



890

891 Figure S2: **A**. Length distributions of cells as determined by phase contrast microscopy. The dotted line
 892 indicates the median of ancestral strain, and the numbers beneath the line names indicate the number of
 893 cells imaged. p-values indicate the results of a t-test when each line is compared to the ancestor. **** $p \leq$
 894 $.0001$, *** $p \leq 0.001$, ** $p \leq 0.01$, * $p \leq 0.05$, ns = not significant. **B**. Distributions of cell volume with
 895 filamentous cells removed (cells with a volume larger than 3x the median for that line). **C**. Increase in
 896 volume is more strongly correlated with cell length compared to cell width. Each dot represents one cell. **D**.
 897 Relationship between the median volume with filaments removed and the total number of molecules of RNA
 898 per CFU. **E**. Correlation between total RNA per CFU for each replicate of each line. **F**. Correlation between
 899 the median cell volumes as determined in this work and cell volumes determined in Grant et al. 2020, figure
 900 5. Error bars indicate the 25th and 75th quantiles of our data.

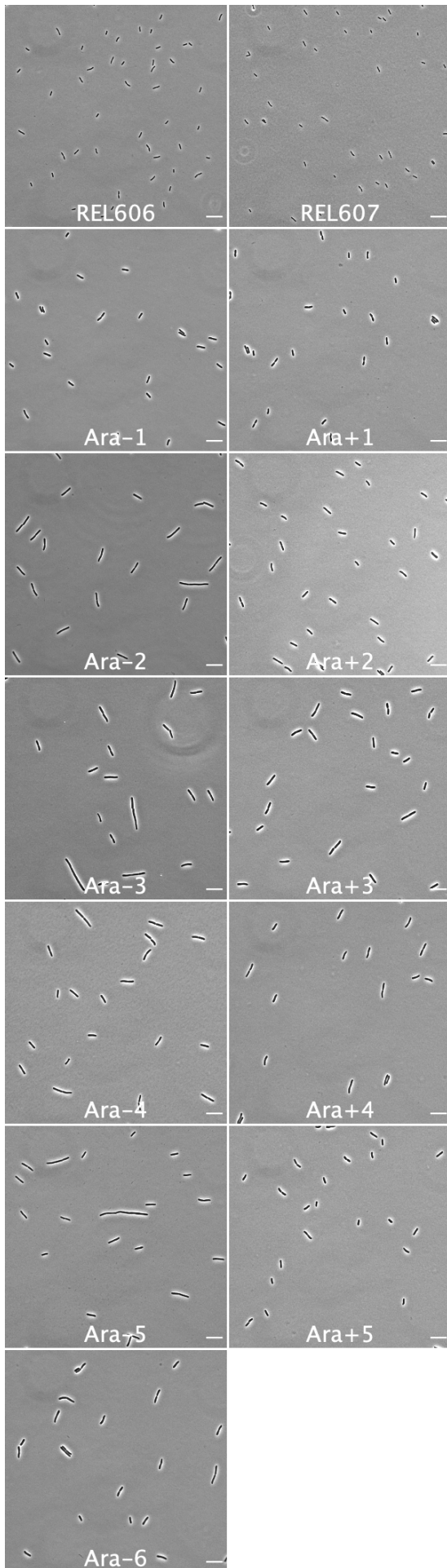
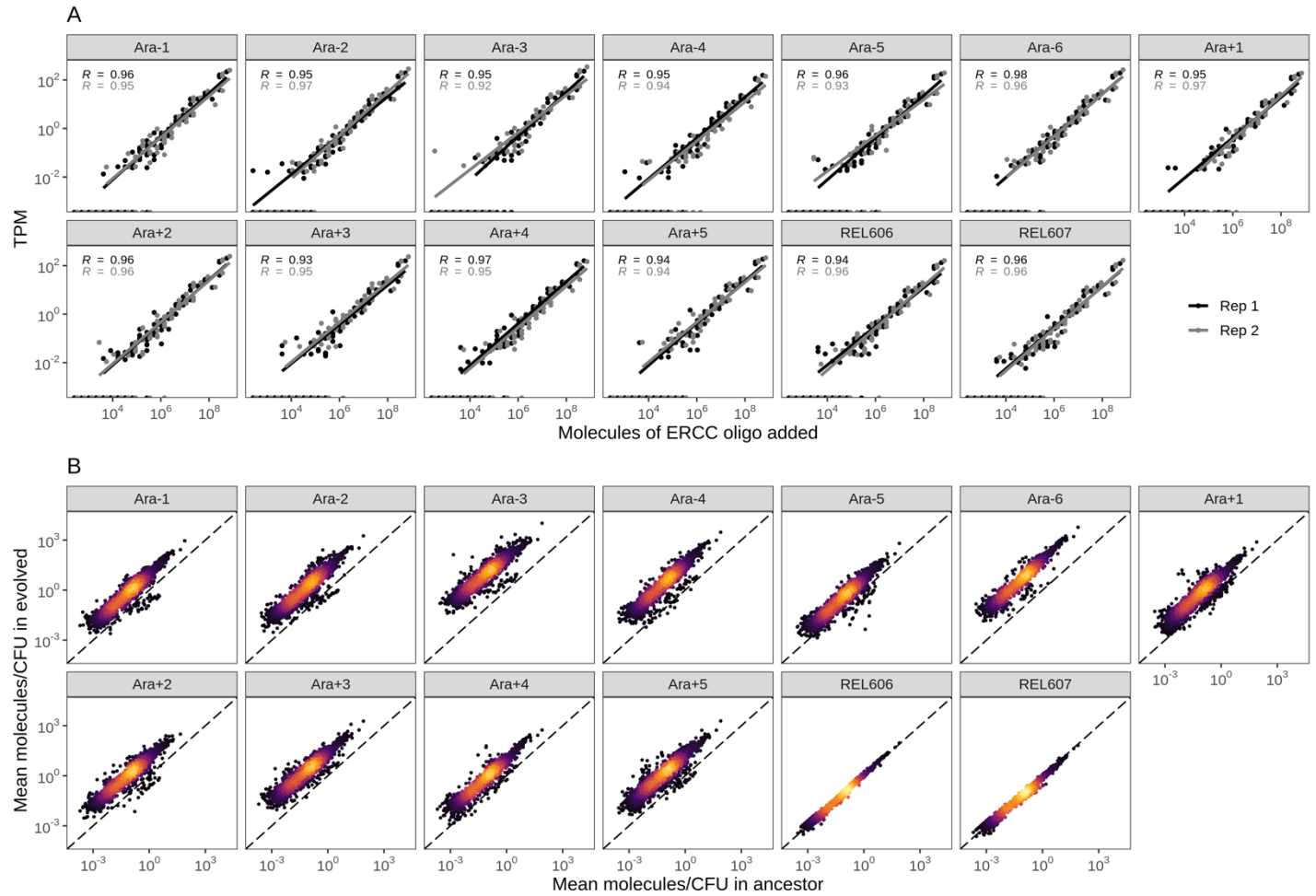
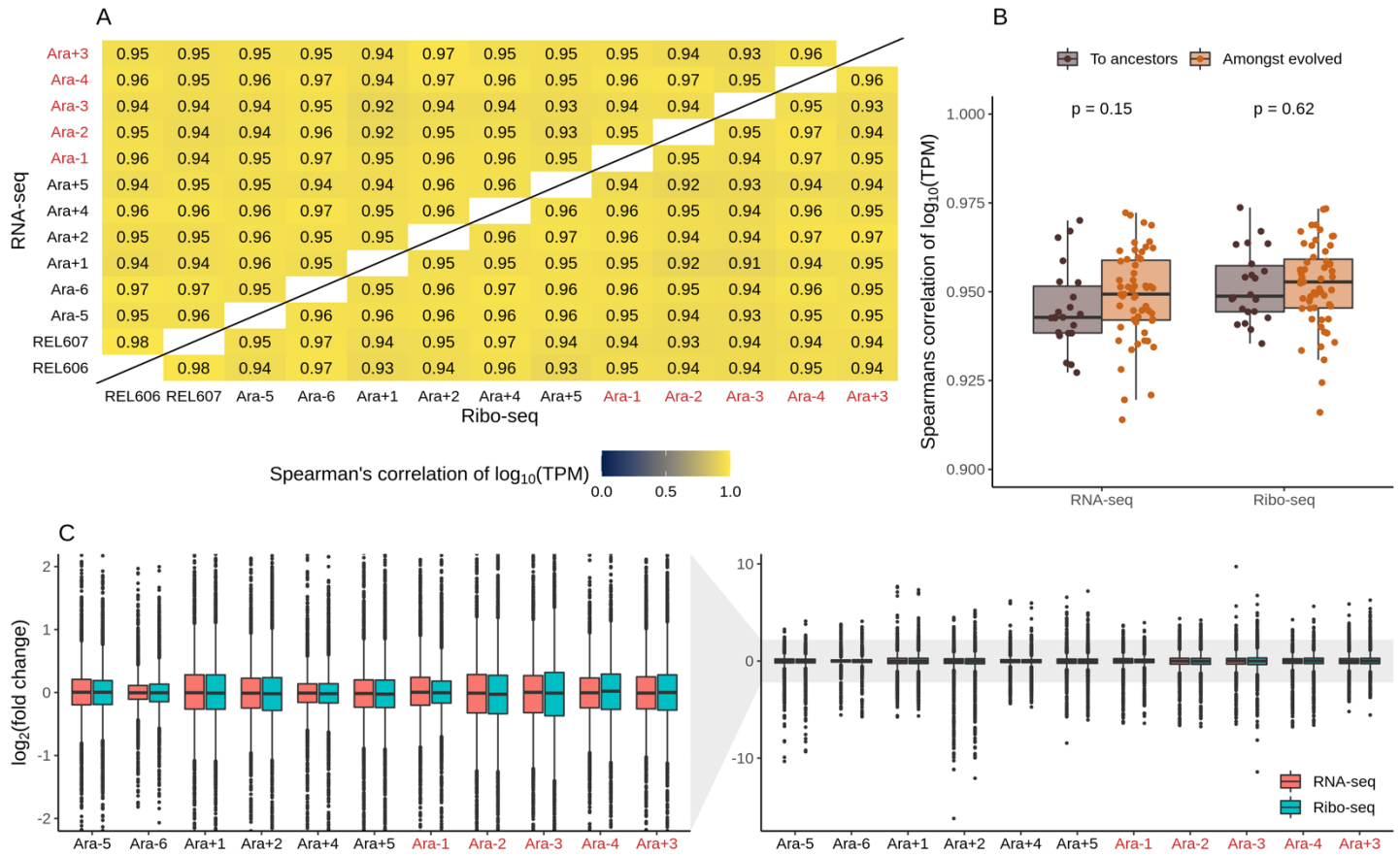


Figure S3: Representative phase contrast images of each of the lines used in this study. Scale bar is 3um.



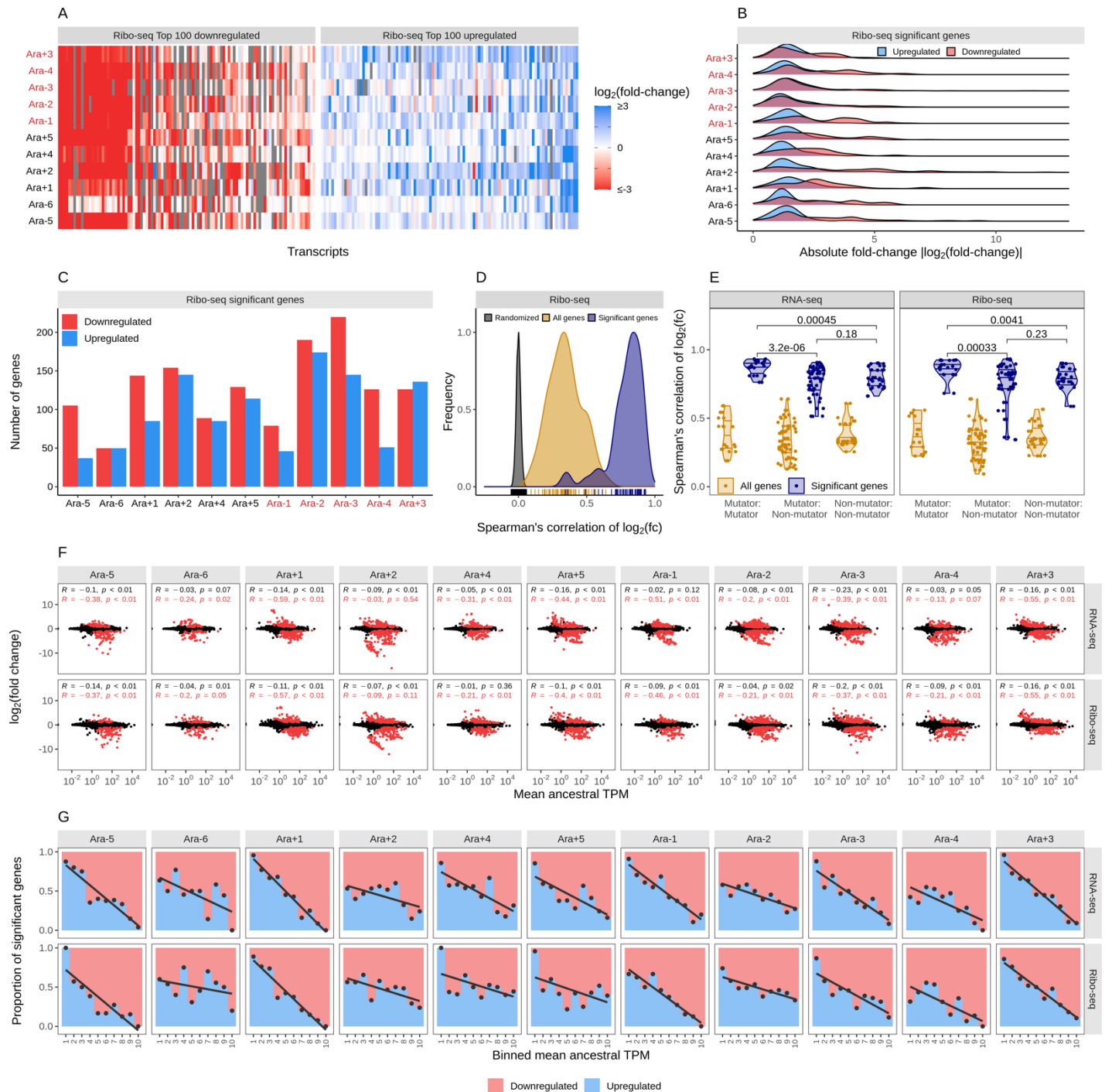
906

907 Figure S4: **A**, linear models relating the number of molecules of each ERCC control sequence added to their
 908 RNA-seq TPM (transcripts per million) in each line. **B**, changes in the absolute number of mRNAs/CFU in
 909 each line relative to the ancestor. The values plotted are the average between 2 replicates of the evolved line
 910 and both replicates from both ancestors (4 in total). **A**. Spike-in RNA control abundances are correlated with
 911 their estimates in sequencing data. Linear models relating the number of molecules of each ERCC control
 912 sequence added to their RNA-seq TPM (transcripts per million) in all RNA-seq samples. **D**. Most genes have
 913 a higher absolute expression in evolved lines. Changes in the absolute number of mRNA molecules per CFU
 914 (colony forming unit) in the 50,000th generation of each line relative to the ancestor. The values plotted are
 915 the average between 2 replicates of the evolved lines and both replicates from both ancestors. REL606 and
 916 REL607 are ancestral strains.



917

918 Figure S5: **A**. Pairwise correlations between expression levels of genes across lines based on $\log_{10}(\text{TPM})$.
 919 The upper triangle shows RNA-seq data, and the lower triangle indicates Ribo-seq data. **B**. Distributions of
 920 pairwise correlations between evolved lines and ancestors (purple) and amongst evolved lines (orange). **C**.
 921 Distributions of all DESeq2 fold-changes for both sequencing methods for all lines. The left panel is a zoom
 922 of the right panel.



923

924

925

926

927

928

929

930

931

932

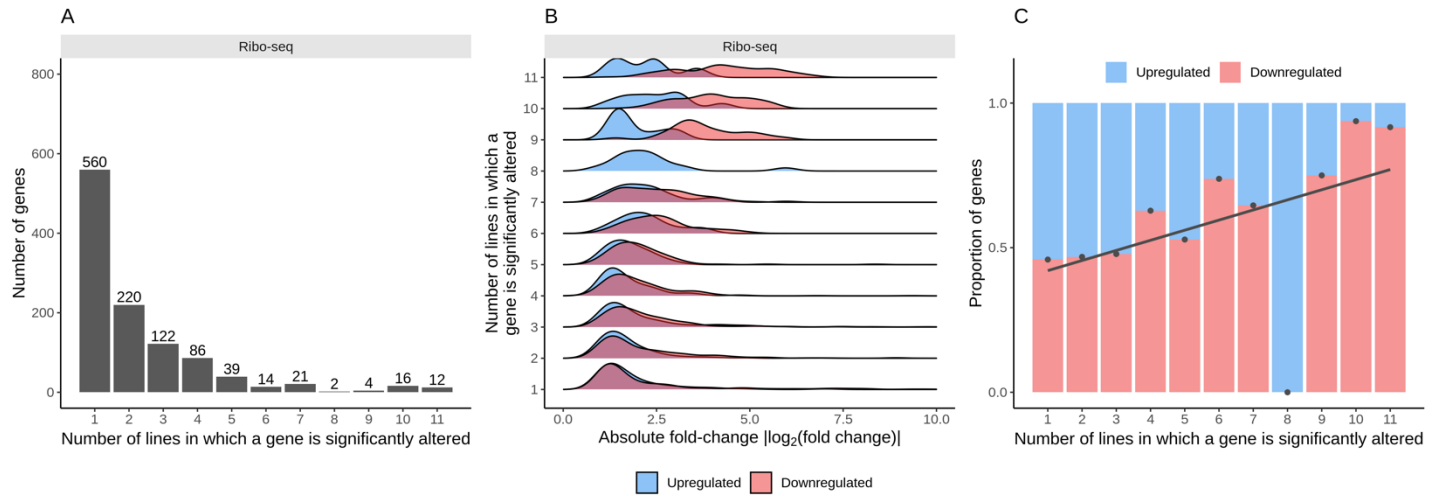
933

934

935

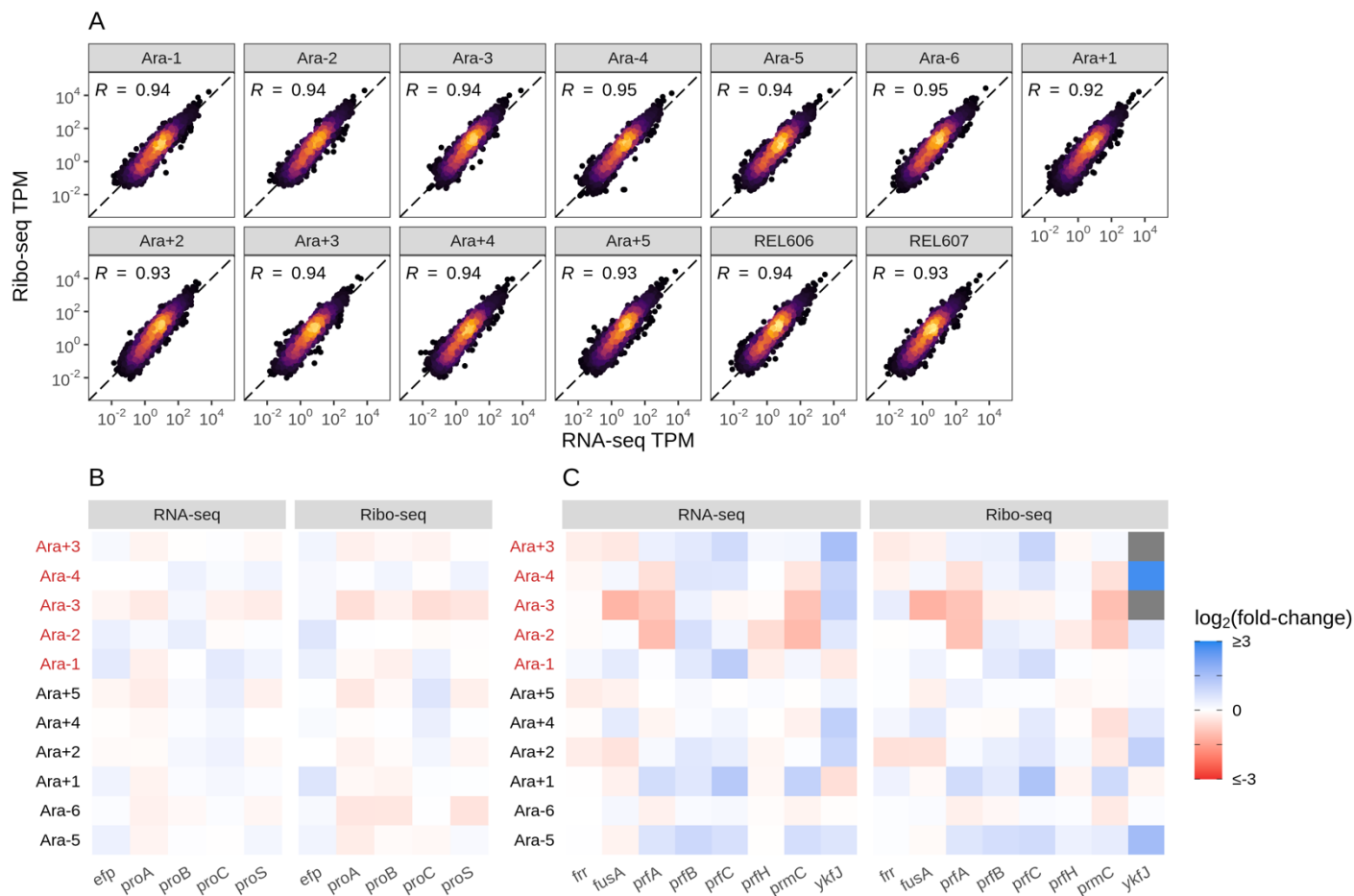
Figure S6: **A**. Parallelism in expression changes across evolved lines. The fold-changes of top 100 down and upregulated genes in each of the lines in the Ribo-seq datasets. Genes are ordered from left to right in order of increasing mean fold-change across evolved lines. Gray bars represent gene deletions. **B**. Downregulated genes have larger effect sizes than upregulated genes. Distribution of statistically significant fold-changes in Ribo-seq data in each line. Statistical significance was based on DESeq2 results using $q \leq 0.01$. **C**. The number of significantly down and upregulated genes in each line. **D**. Pairwise correlations of evolved lines based on all (yellow curve) or statistically significant (blue curve) Ribo-seq fold-changes. Each of these curves is significantly different from a distribution based on correlations made after randomizing the fold-changes (grey curve) within each line ($p \leq 0.01$, t-test). **E**. Pairwise-correlations between fold-changes in expression levels of genes based on their mutator status. **F**. Fold-changes in expression levels of genes in evolved lines scale negatively with their ancestral expression levels. The relationship between ancestral TPM in both RNA- and Ribo-seq datasets corresponding fold-changes across all lines. The black dots represent all the points

936 (all genes), and the red dots represent significantly altered genes. **G.** Genes with high ancestral expression
937 are typically downregulated. The panel shows the proportion of differentially expressed genes that are
938 up/down-regulated as a function of ancestral expression (TPM).



939

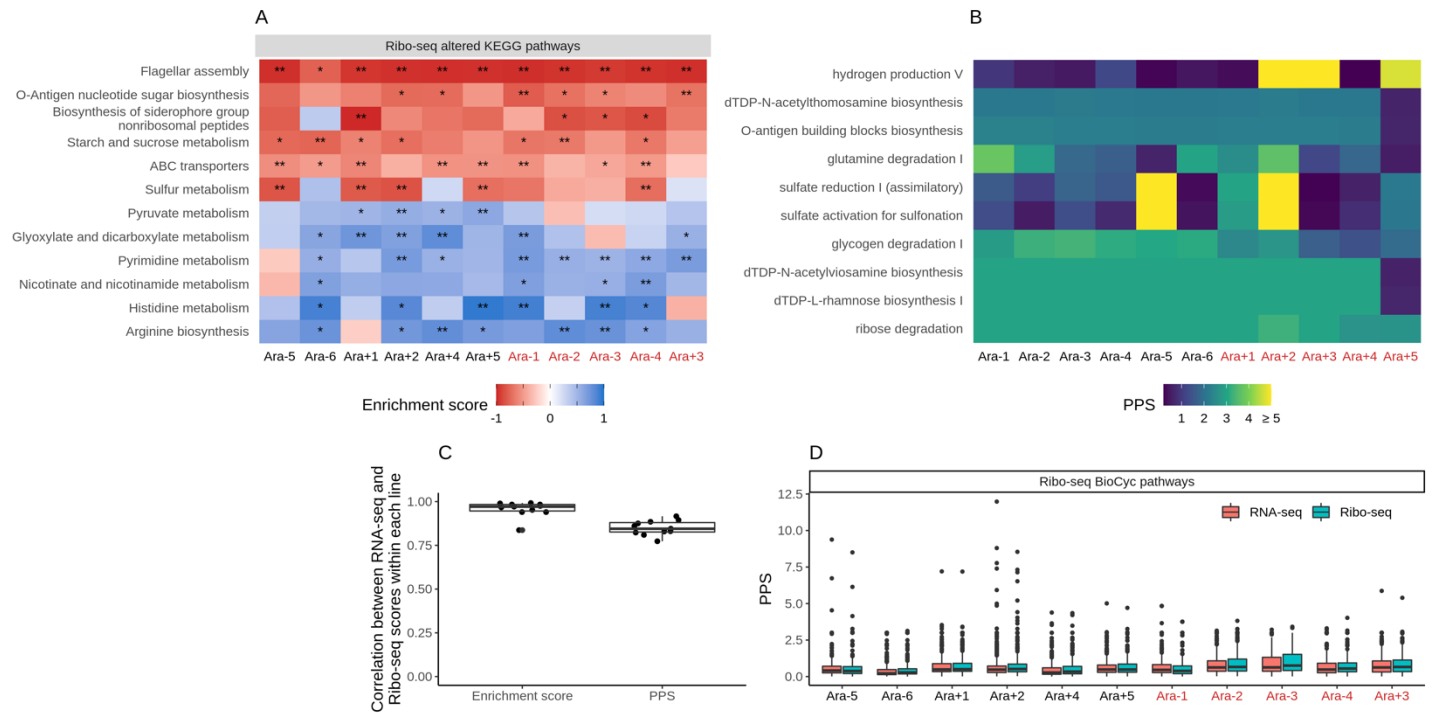
940 Figure S7: **A**. The number of evolved lines in which a gene's expression level was significantly altered ($q \leq$
941 0.01) was based on the DESeq2 results for the Ribo-seq dataset. **B**. Frequency downregulated genes have
942 larger effect sizes than upregulated genes. Distributions of the Ribo-seq fold-changes for the genes. **C**.
943 Frequently altered genes are typically downregulated. The proportion of up and downregulation of genes in
944 the Ribo-seq dataset as a function of their frequency of expression changes across lines.
945



946

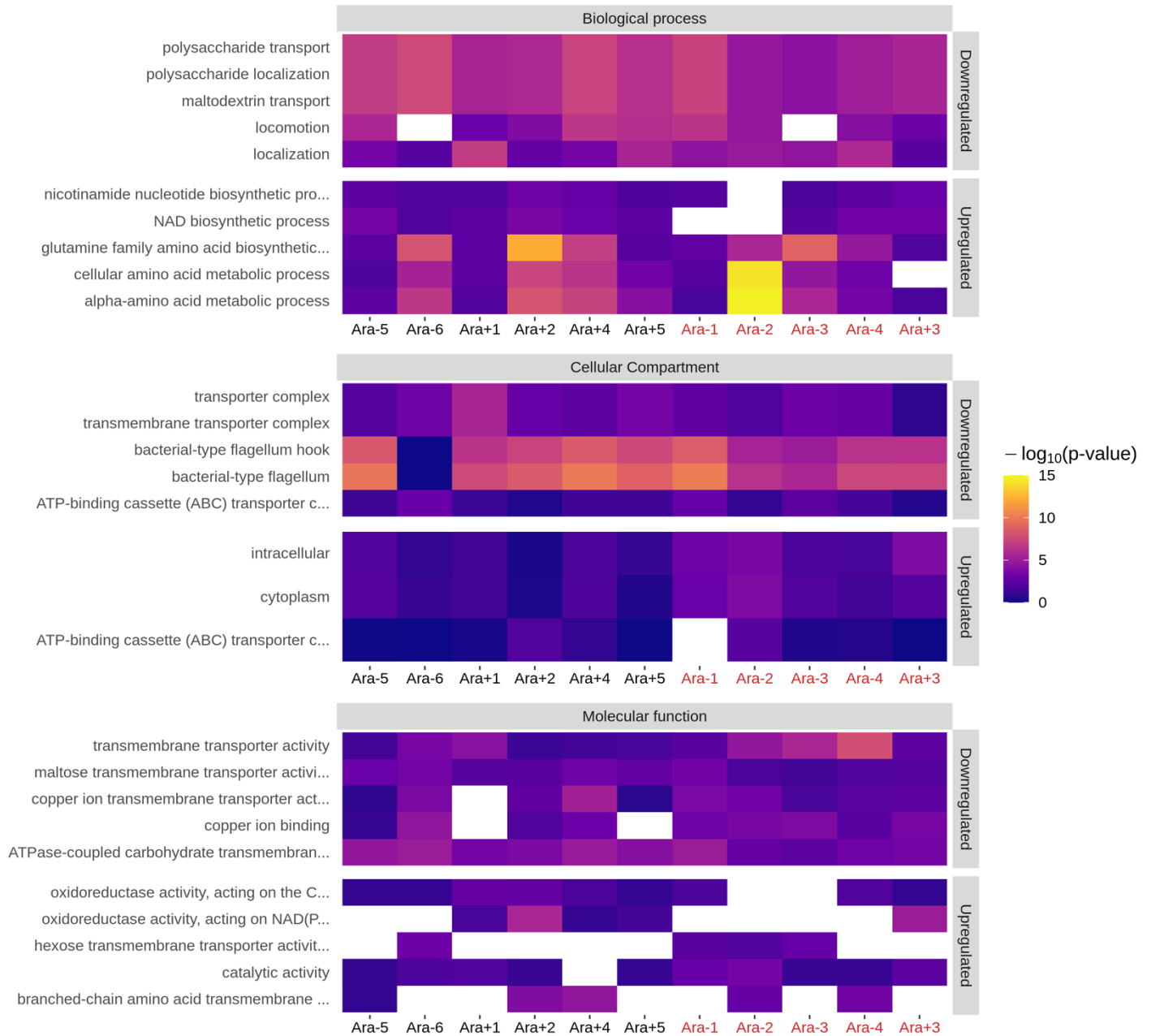
947 Figure S8: **A**. Translational changes are positively correlated with transcriptional changes. The relationship
948 between RNA-seq and Ribo-seq TPM across all evolved lines. The TPMs are averaged between the
949 replicates. **B**. Fold-changes in expression levels of genes involved in proline biosynthesis. **C**. Fold-changes
950 in expression levels of translation termination factors and related genes.
951

952



953

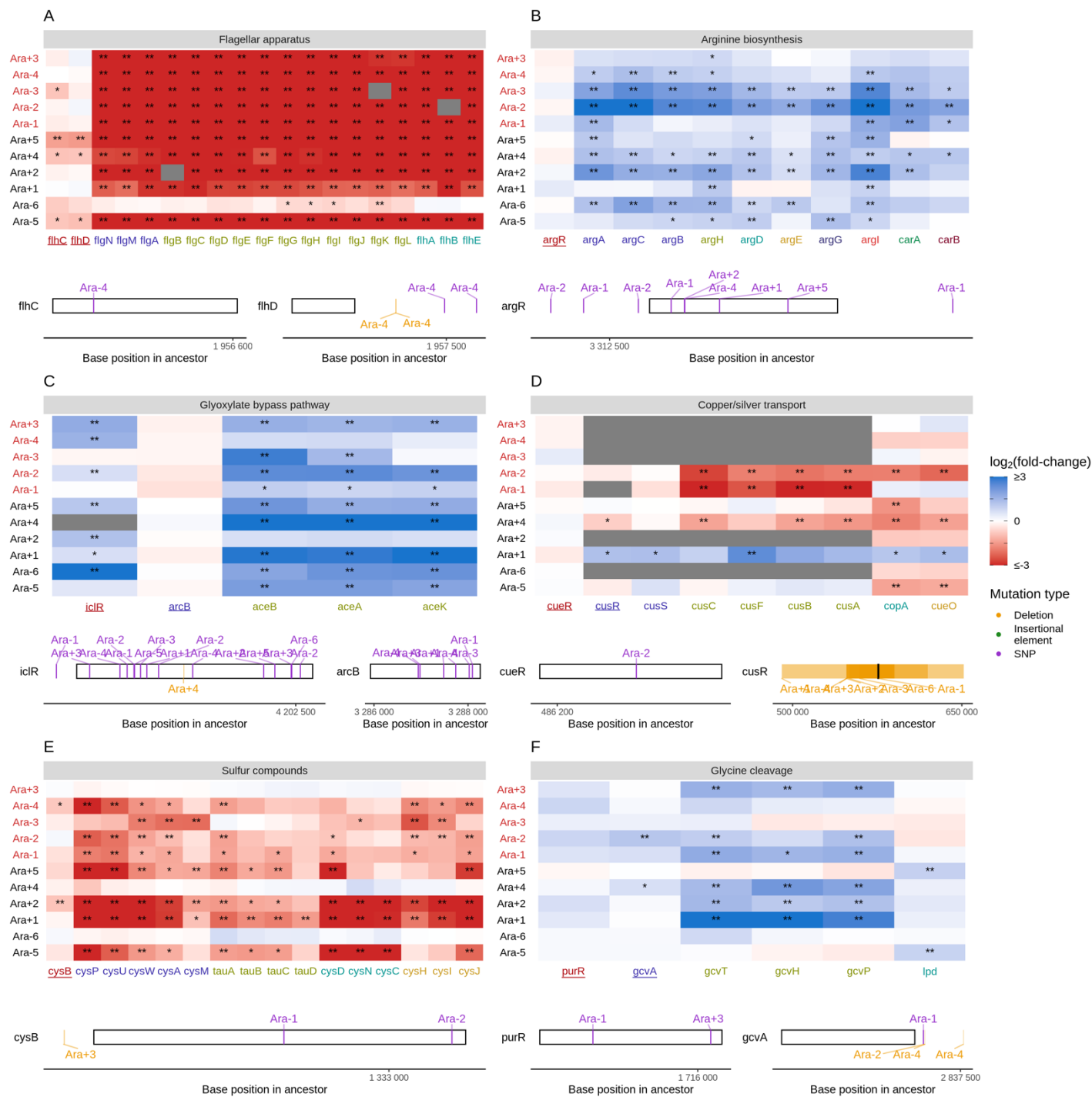
954 Figure S9: **A**. Parallel changes in functional categories. KEGG enrichment scores from the Ribo-seq data.
 955 Enrichment score represents the degree to which a pathway was up (positive) or downregulated (negative).
 956 Functional categories are ordered by increasing mean enrichment score across the lines. Enrichment score
 957 represents the degree to which a pathway was up (positive) or downregulated (negative). **B**. Pathway
 958 perturbation score (PPS) calculated from Ribo-seq fold changes. Higher PPS indicates larger degrees of
 959 alteration but does not indicate directionality. **C**. Pairwise correlations of KEGG enrichment scores for all
 960 pathways that were significantly altered in at least one line. **D**. Distribution of PPS scores in both RNA-seq
 961 and Ribo-seq datasets across all lines.



962

963 Figure S10: The top 5 up and downregulated GO categories for each ontology term. For each ontology, only
 964 terms with a p-value ≤ 0.01 based on Fisher's exact test in at least 4 lines were considered. White spaces
 965 indicate that a particular category was not significantly altered in a line.

966



967

968 Figure S11: **A-F**. Mutations in transcriptional regulators lead to parallel changes in gene expression (RNA-
 969 seq). Gene names in each category are colored based on their operon membership. Transcription factors for
 970 each class of genes are underlined. Asterisks indicate statistical significance of fold-changes, ** $q \leq 0.01$, * q
 971 ≤ 0.05 . Grey panels in the heatmap indicate gene deletion. Lower panels show the type and location of
 972 mutations in each transcription factor.
 973
 974
 975
 976
 977